Soft Matter

ROYAL SOCIETY OF CHEMISTRY

PAPER

View Article Online
View Journal | View Issue

Cite this: *Soft Matter*, 2023, **19**, 8802

Trapped tracer in a non-equilibrium bath: dynamics and energetics

Koushik Goswami *[a] and Ralf Metzler *[ab]

Received 2nd September 2023,
Accepted 1st November 2023

DOI: 10.1039/d3sm01177a

rsc.li/soft-matter-journal

We study the dynamics of a tracer that is elastically coupled to active particles being kept at two different temperatures, as a prototype of tracer dynamics in a non-equilibrium bath. Employing analytical techniques, we find the exact solution of the probability density function for the effective motion of the tracer. The analytical results are supported by numerical simulations. By combining the experimentally accessible quantities such as the response function and the power spectrum, we measure the non-equilibrium fluctuations in terms of the effective temperature. In addition, we compute the energy dissipation rate to find the precise effects of activity. Our study is relevant in understanding athermal fluctuations arising in cytoskeletal networks or inside a chromosome.

1 Introduction

The dynamics of a test particle inside a living cell is a complex process,[1–3] and it often occurs in a regime where the laws of equilibrium physics cannot be applied, or in other words, the detailed balance condition breaks down and the usual fluctuation–dissipation theorem (FDT) is violated.[1,4] In systems, in which the FDT holds, the response function of a system where the influence of an external force acts is related to its spontaneous fluctuations *via* the ambient temperature.[5–7] Employing microrheology and single-particle tracking techniques, it is possible to measure the fluctuations of a tracer trapped in a medium and thus check the validity of the FDT.[8–10] Any deviation from the usual FDT indicates a non-equilibrium nature of the observed dynamics, found earlier in a wide class of systems, *e.g.*, aging glasses,[11,12] sheared materials,[13,14] externally driven colloids,[15,16] active matter,[17,18] and others.[1,19–21] Based on the knowledge from equilibrium physics, a generalised version of the FDT was proposed,[22–27] and the notion of an effective temperature is introduced in the theorem as a substitute for the ambient temperature.[28–35] Thus one can characterise the fluctuations and estimate the deviations from equilibrium by correlating useful quantities extracted from experimental data such as the response function and the power spectral density (PSD).[10,36,37] In the context of active matter, there have been several experimental as well as theoretical and simulation-based studies which have validated the generalised approach to the FDT by incorporating the concept of effective temperature, and quantified the departure from equilibrium.[38,39,41–50]

An emerging area of biophysical research is to understand how the activity affects biological processes in a living cell. The shape of a cell is formed by the cytoskeleton—an active viscoelastic network (gel) of cross-linked filaments and motor proteins.[32,51–53] Harnessing energy from ATP hydrolysis, motors generate force along the filaments, a phenomenon which renders the network dynamic and drives it out of equilibrium.[1,54] Naturally, a probe particle immersed inside the network exhibits distinct dynamical properties such as enhanced diffusion and a non-Boltzmann distribution of displacements as observed in numerous experiments.[1,4,45,55,56] Measuring the mechanical and dynamic properties, it was observed that the probe's position varies non-monotonically with time due to compression and eventual relaxation of the network controlled by motor activity.[1] For such a system, a clear violation of the FDT was demonstrated, and the effect was particularly prominent at low frequencies of the PSD at which enhanced fluctuations of the probe's displacement occur. Similar observations were reported in activity-induced flickering of membranous systems such as red blood cells, cell nuclei, vesicles, *etc.*[9,29–31] In these systems, a viscoelastic network made up of a cytoskeletal protein (spectrin) constitutes the cell membrane (of red blood cells), and rearrangements of the network due to metabolic activity cause athermal fluctuations of the membrane.[29,57]

With high-resolution imaging techniques recent investigations have revealed the effects of ATP-powered activity on the dynamics of chromatin which resides inside the cell nucleus.[32,58,59] For instance, several studies have observed the coherent motion of chromatin with long-range spatial correlations due to the directional force generated by nuclear enzymes.[59,60] The shape of the nucleus is determined by the

[a] *Institute of Physics & Astronomy, University of Potsdam, 14476 Potsdam-Golm, Germany. E-mail: goswamikoushik10@gmail.com*
[b] *Asia Pacific Centre for Theoretical Physics, Pohang 37673, Republic of Korea. E-mail: rmetzler@uni-potsdam.de*

surrounding membrane called the nuclear envelope, which separates the nuclear contents such as chromatin and the nucleoplasm from the remaining cellular cytoplasm. Therefore the undulations of the nuclear shape are controlled by two kinds of activity—from outside by the cytoskeleton and from inside by the chromatin that is actively remodelled continuously.[61] A recent experiment suggested that these activities act differently on the shape fluctuations; particularly, cytoskeletal activity amplifies the fluctuations, while these are dampened if chromatin is involved.[32]

To explain the properties of non-equilibrium fluctuations of the above examples, the systems are generally modelled as the coupled motion of a tracer and surrounding bath particles, where the tracer represents the probe or membrane while the bath particles correspond to faster degrees of freedom which account for activity.[40,41,62–64] Integrating out the faster degrees of freedom, one can obtain the effective motion of the tracer. We note that, to capture the collective effects on the dynamics, the environment is often modelled as a polymeric network which can cause subdiffusive motion of the tracer due to the viscoelastic feedback from the environment.[65] Along this direction, extensive studies have been carried out.[65–71]

Here we consider a minimal model (analogous to those used in ref. 41 and 63) to describe the viscoelasticity of the environment. The advantage of using this model is that we can apply an exact analytic theory to investigate the basic elements of tracer diffusion in a non-Markovian active environment with specific kind of viscous and elastic components, and to get insights into the energetics. To keep things simple, we consider harmonic couplings between the tracer and the bath particles, while there is no interaction among the bath particles. In this setting, an individual tracer particle itself is assumed to undergo normal diffusion, *i.e.*, it is driven by a Gaussian white noise. Even with this simple assumption, the tracer's dynamics can no longer be described in the equilibrium framework, rather it is characterised by an effective temperature which is a clear indicator of the non-equilibrium nature.[41] This model can thus capture enhanced fluctuations of the tracer, but it fails to characterise the medium which is itself intrinsically active or the one where enhanced activity reduces non-equilibrium fluctuations.[32]

To address the second problem, a modification of the existing model was proposed recently by considering a coupling of the tracer to a mixture of hot and cold particles.[63] Note that a similar model was used earlier to explore several interaction-mediated phenomena.[72–75] One important trait of an active particle is the persistence of its motion over a finite timescale called persistence time, which is missing in the mentioned studies.[17,26,33,76,77] Manifestations of active matter are, in fact, prevalent everywhere—in swimming bacteria, migrating cells to schooling of fish and flocking of birds.[78–81] Other realisations where the influence of activity can be found are facilitated looping of a passive polymer in the presence of active bath particles, enhanced long-range coordination between enhancers and promoters in gene regulation, *etc.*[82–85]

An analytically tractable description of active system is the active Ornstein–Uhlenbeck particle (AOUP) model which introduces a correlation time to the particle dynamics described within a Gaussian regime.[33,47,86] Recently, a few theoretical and simulation-based studies considered the fluctuating motion of a passive tracer in an active medium by modelling the bath particles as AOUPs.[62,87–90] For example, the authors of ref. 89 modelled a Stirling-like heat engine in a viscoelastic active bath by considering the system as a large passive tracer interacting with the AOUPs *via* harmonic potentials. Using this model, they analytically determined the viscoelastic effects on the steady-state properties and engine efficiency in the quasi-static limit. In ref. 90, a similar setup was established through computer simulations, where an active medium consisting of smaller active disks interacted with each other and with a confined tracer *via* repulsive Lennard-Jones-type potentials. The effective motion of the tracer was found to be influenced by the interplay between the activity of the medium and the tracer's relaxation dynamics.

In this paper, we present a generalisation of the standard model presented in ref. 41 and 63, which encompasses most of its variations mentioned above, namely, the stochastic motion of a tracer confined in a harmonic potential and interacting with bath particles *via* elastic bonds; the bath particles at two different temperatures are driven by either white or coloured Gaussian noises. We develop an analytical scheme which solves the problem exactly, and the approach can be extended easily to incorporate other models of active noise. Also, it can be applied to study the fluctuating dynamics of an active tracer, a tracer with inertia, and bath particles subjected to both active and thermal noise. It is important to note that, for a comprehensive modelling of an active particle, one would typically include additional thermal driving in the dynamics of bath particles.[91,92] However, for the purposes of this study, we choose to omit thermal effects on the bath particles to focus exclusively on the impact of active contributions. Furthermore, it is essential to underscore that the influence of active noise significantly outweighs thermal contributions in the hot-cold mixture model of active bath particles. Active particles are assumed to be connected to reservoirs separate from the tracer, allowing us to safely disregard thermal effects on the active particles while still assessing their influence on the tracer.

The plan of the paper is as follows. In Section 2, we present the details of the model. For this model, the standard dynamical observables such as the mean squared displacement (MSD) and the probability density function (PDF) of the displacement are provided in Section 3. In Section 4, we derive the exact results for the relevant thermodynamic quantities to quantify non-equilibrium fluctuations. Additionally, we establish a generalised FDT by defining a frequency-dependent effective temperature, and we investigate stochastic energetics by calculating the amount of energy exchanged between the system and the environment. We summarise our results in Section 5. Other important details to supplement the main results are presented in subsequent appendices: Appendix A is dedicated to the exact derivation of the PDF. The simulation details of the model are discussed in Appendix B. In Appendix C, we present the detailed derivations of the response function and the autocorrelation. All the quantities and parameters used in the text are collected in Table 1.

Table 1 Notations and dimensions of quantities/parameters used in the text

Notation	Description	Unit
x, x_h, x_c	Respective positions of tracer, hot and cold particles	μm
t, Δt	Total time and time step	s
τ_h, τ_c	Respective persistence times of hot and cold particles	s
γ_{tr}, γ_b	Friction coefficients of tracer and active bath particles	pN μm^{-1} s
λ	Strength of external harmonic trap	pN μm^{-1}
λ_0	Strength of interaction potential between tracer and active particles	pN μm^{-1}
$1/k$	Relaxation time of tracer in external harmonic trap	s
$1/k_I$	Interaction timescale of tracer interacting with bath particles	s
$1/k_0$	Interaction timescale of active bath particles interacting with tracer	s
D_{tr}, D_h, D_c	Respective diffusivities of tracer, hot and cold particles in model II	μm^2 s^{-1}
D_{tr}, $D_{h,m}$, $D_{c,m}$	Respective diffusivities of tracer, hot and cold particles in model III	μm^2 s^{-1}
G_h, G_c	Amplitudes of active forces acting on hot and cold particles in model III	μm^2 s^{-2}
D_{eff}, $D_{h,eff}$, $D_{c,eff}$	Respective effective diffusivities of tracer, hot and cold particles	μm^2 s^{-1}
T_{tr}, T_h, T_c	Temperatures of tracer, hot and cold particles	K
T_{eff}, $T_{act,h}$, $T_{act,c}$	Effective temperatures of a single tracer, hot and cold particles	K
N_h, N_c	Numbers of hot and cold particles	1
$\chi(t)$	Response function [eqn (11)]	1
$\tilde{\mathbb{S}}_{xx}(\omega)$	Power spectral density of x [eqn (16)]	μm^2 s
k_B	Boltzmann constant	pN μm K^{-1}
$E_{act}(\omega)$	Active energy [eqn (21)]	pN μm
$\langle J \rangle$	Energy dissipation rate [eqn (24)]	pN μm s^{-1}
α_1	Eqn (35)	s^{-1}
α_2	Eqn (36)	s^{-2}
t_s, t_l	Eqn (13a) and (13b)	s
χ_s, χ_l	Eqn (13c) and (13d)	1
α_{11}, α_{12}	Eqn (27a) and (27c)	s^{-2}
α_{21}, α_{22}	Eqn (27b) and (27d)	K
$\phi(t)$	Eqn (33)	1
$\psi(t)$	Eqn (34)	s

2 Model

Suppose that a tracer particle is immersed in a bath consisting of two types of active particles: one, N_h of active particles are in contact with thermostats of higher temperature T_h. Two, N_c cold particles are driven by a thermostat with temperature T_c, where $T_c \leq T_h$, and we take $N = N_h + N_c$. We assume that the active particles do not interact with each other, and as a simple but effective approximation, the tracer is coupled to all these particles *via* harmonic potentials of the same strength λ_0. On top of those interactions, the tracer is confined in an external harmonic potential of strength λ, *e.g.*, exerted by an optical or acoustic trap.[66,93–95] In addition, it is subjected to white Gaussian noise arising due to collisions with solvent particles kept at temperature T_{tr}. This description is sketched in Fig. 1. Considering the isotropic nature of the medium, it is sufficient to deal with a one-dimensional system as the procedure can easily be extended to higher dimensions.

In a minimal model, the governing equations for the coupled dynamics of the tracer (with coordinate x) and the active particles (with coordinate x_h and x_c for hot and cold particles, respectively) in the overdamped limit can be expressed as[41,63]

$$\dot{x}(t) = -kx(t) - \sum_{i=1}^{N_h} k_I(x(t) - x_{h,i}(t)) - \sum_{i=1}^{N_c} k_I(x(t) - x_{c,i}(t)) + \eta(t), \quad (1a)$$

$$\dot{x}_h(t) = -k_0(x_h(t) - x(t)) + \eta_h(t), \quad (1b)$$

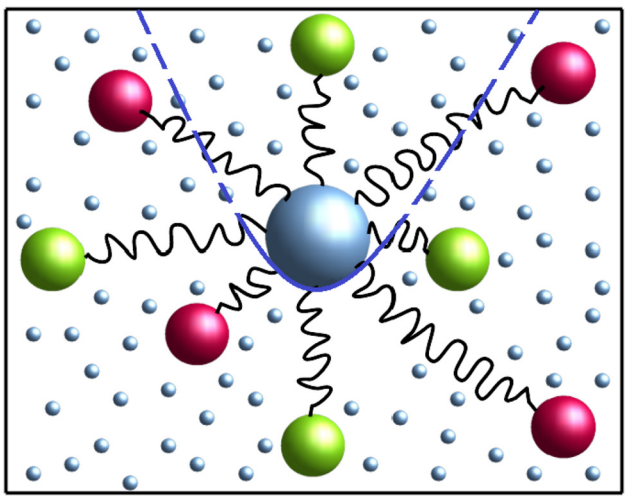

Fig. 1 Illustration of a tracer particle (blue sphere in the centre) confined in a harmonic trap of strength in a bath comprising hot (red) and cold (green) particles. The tracer is coupled to the particles *via* harmonic springs of strength λ_0. In addition, it is surrounded by solvent molecules (small blue spheres) which act as the source of thermal fluctuations.

$$\dot{x}_c(t) = -k_0(x_c(t) - x(t)) + \eta_c(t). \quad (1c)$$

Here the dot symbol above the variable denotes its time derivative. The above set of equations has been rescaled by the friction coefficients of the particles, and thus the strength of the potentials are redefined as $k = \lambda/\gamma_{tr}$, $k_I = \lambda_0/\gamma_{tr}$, and $k_0 = \lambda_0/\gamma_b$, where γ_{tr} and γ_b are the friction coefficients of the tracer and the

active particles, respectively. The term η in eqn (1a) represents zero-mean, white Gaussian noise corresponding to the thermal fluctuations acting on the tracer, with $\langle\eta(t)\rangle = 0$ and $\langle\eta(t)\eta(t')\rangle = 2D_{\rm tr}\delta(t-t')$, where the diffusivity of the tracer $D_{\rm tr}$ is related to the bath temperature $T_{\rm tr}$ *via* the Einstein–Smoluchowski–Sutherland relation $D_{\rm tr} = (k_{\rm B}T_{\rm tr})/\gamma_{\rm tr}$, with the Boltzmann constant $k_{\rm B}$.[96] From now on, we set $k_{\rm B} = 1$. For the active particles, we consider two different models for the active noises $\eta_{\rm h}$ and $\eta_{\rm c}$ which are discussed in the following.

2.1 Active noise models

Eqn (1b) and (1c) describe the dynamics of active hot and cold particles which are subject to the noises $\eta_{\rm h}$ and $\eta_{\rm c}$, respectively. For simplicity, we consider that all hot (or cold) particles follow similar dynamical properties, but they do not interact with each other. So the autocorrelation function of noises $\eta_{{\rm h},i}$ and $\eta_{{\rm c},j}$ acting on the ith hot particle and jth cold particle is given by

$$\langle\eta_{{\rm h},i}(t_1)\eta_{{\rm c},j}(t_2)\rangle = \delta_{\rm hc}\delta_{ij}\kappa(|t_1-t_2|), \tag{2}$$

with $\kappa(|t|)$ being the autocorrelation function with the time-translational invariance, and δ_{ab} the Kronecker delta of any two variables a and b.

2.1.1 Model I: active particles driven by Gaussian white noises. Let us first consider a simple model where the active particles just act as a source of additional energy input to the tracer dynamics, and for such a case, the noises in (2) are considered as white Gaussian with zero mean and delta correlations,[97]

$$\langle\eta_{{\rm h},i}(t)\eta_{{\rm h},j}(t')\rangle = 2D_{\rm h}\delta_{ij}\delta(t-t') \tag{3a}$$

$$\langle\eta_{{\rm c},i}(t)\eta_{{\rm c},j}(t')\rangle = 2D_{\rm c}\delta_{ij}\delta(t-t') \tag{3b}$$

where $D_{\rm h}$ and $D_{\rm c}$ are the diffusivities of hot and cold particles, respectively, defined as $D_{\rm h} = k_{\rm B}T_{\rm h}/\gamma_{\rm b}$ and $D_{\rm c} = k_{\rm B}T_{\rm c}/\gamma_{\rm b}$. In the long-time limit, each particle attains an equilibrium state, thereby assuming a Boltzmann distribution.

2.1.2 Model II: active particles driven by Gaussian coloured noises. In contrast to the previous model, here we characterise the active particles by the persistence properties of their motion, or in other words, finite correlation times denoted as $\tau_{\rm h}$ and $\tau_{\rm c}$ are included in the dynamics of the hot and cold particles. As a common yet effective model, the active noises $\eta_{\rm h}$ and $\eta_{\rm c}$ are described by the Ornstein–Uhlenbeck process (OUP),[33,86]

$$\dot\eta_{\rm h}(t) = -\frac{1}{\tau_{\rm h}}\eta_{\rm h}(t) + \frac{1}{\tau_{\rm h}}\eta_{\rm w,h}, \tag{4a}$$

$$\dot\eta_{\rm c}(t) = -\frac{1}{\tau_{\rm c}}\eta_{\rm c}(t) + \frac{1}{\tau_{\rm h}}\eta_{\rm w,c}, \tag{4b}$$

where $\eta_{\rm w,h}$ and $\eta_{\rm w,c}$ represent Gaussian white noises. Thus the autocorrelation functions of the active noises $\eta_{\rm h}(t)$ and $\eta_{\rm c}(t)$ can be expressed as

$$\langle\eta_{{\rm h},i}(t)\eta_{{\rm h},j}(t')\rangle = \frac{D_{\rm h}}{\tau_{\rm h}}\delta_{ij}\exp\left(-\frac{|t-t'|}{\tau_{\rm h}}\right), \tag{5a}$$

$$\langle\eta_{{\rm c},i}(t)\eta_{{\rm c},j}(t')\rangle = \frac{D_{\rm c}}{\tau_{\rm c}}\delta_{ij}\exp\left(-\frac{|t-t'|}{\tau_{\rm c}}\right). \tag{5b}$$

Therefore, each free active particle can reach a steady state after its correlation time, and its distribution is of Boltzmann form, yet involves effective diffusivities given by $D_{\rm h,eff} = \dfrac{D_{\rm h}}{1+k_0\tau_{\rm h}}$ and $D_{\rm c,eff} = \dfrac{D_{\rm c}}{1+k_0\tau_{\rm c}}$ for the hot and cold active particle, respectively.[35] Such a description is often referred to as the active Ornstein–Uhlenbeck particle (AOUP) model. Note that in the limit $\tau_{\rm h} \to 0$ (or $\tau_{\rm c} \to 0$), the active noise becomes delta-correlated white noise, and thus one recovers the previous model.

A related model is the modified AOUP (MOUP) in which the correlations for the active noises have similar forms as in (5a) and (5b), but the amplitudes do not depend on the correlation times, *i.e.*, the terms $D_{\rm h}/\tau_{\rm h}$ and $D_{\rm c}/\tau_{\rm c}$ are replaced by the fixed amplitudes $G_{\rm h}$ and $G_{\rm c}$.[77] The MOUP will be considered as model III. In model III, the diffusivities of a hot and a cold particle can be defined as $D_{\rm h,m} = G_{\rm h}\tau_{\rm h}$ and $D_{\rm c,m} = G_{\rm c}\tau_{\rm c}$, respectively, implying their dependence on persistence times. However, it is worth noting that for fixed values of diffusivities, both model II and model III yield the same result for the dynamical properties.

3 Dynamical properties

To get an idea about the dynamics of the tracer, we find the PDF of the displacement and the MSD of the tracer for the above models. A complete derivation of the PDF is shown in Appendix A. The results are used below for the detailed analysis.

From eqn (50), the MSD defined as $\langle[x(t)-\langle x(t)\rangle]^2\rangle$ is derived in Appendix A. Given that the mean of the distribution is zero (*i.e.*, $\langle x(t)\rangle = 0$), we will henceforth refer to the MSD as $\langle x(t)^2\rangle$. The MSD is displayed in Fig. 2. Fig. 3 shows the PDF (48) of the tracer displacement x for the two models of active particles at different times, and we notice that the distribution is always Gaussian. However, the width of the PDF varies non-monotonically with time, corresponding to the MSD behaviour captured in Fig. 2. At $t = 0$, there is no effective interaction between the tracer and the active particles as the tracer is in equilibrium at temperature $T_{\rm tr}$, and thus it is Gaussian of width $\langle x(0)^2\rangle = \dfrac{T_{\rm tr}}{\lambda}$ (see Appendix A). At short times, the tracer motion then becomes constrained due to the coupling to the active particles. This is evident from the short-time behaviour $\langle x(t)^2\rangle \sim -j(N_{\rm h}+N_{\rm c})k_I t$, suggesting that the initial decrease of the MSD depends on the coupling strength and the number of active particles that are elastically coupled to the tracer. After an intermediate time $t^\star$, the MSD starts increasing and reaches a plateau value in the long-time limit. This behaviour can be attributed to the relaxation of the system to a steady state by exchanging energy with the active particles. Note that a similar variation of the displacement was observed experimentally for a probe diffusion inside a cytoskeletal network.[1] In the long-time

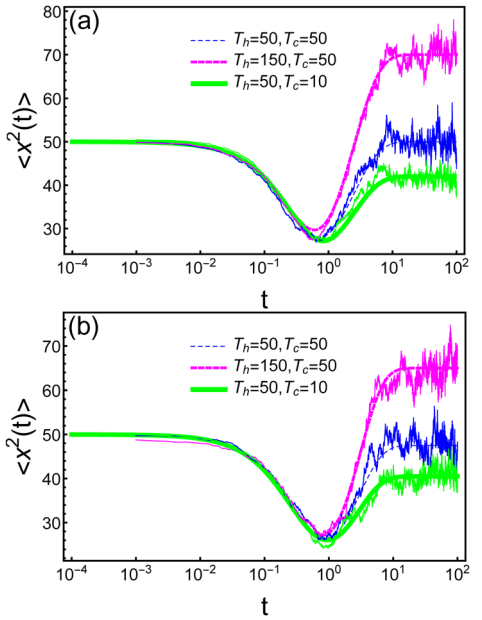

Fig. 2 Log–linear plot of the second central moment of the displacement *versus* time for (a) model I and (b) model II at different temperatures of the hot and cold particles. The theoretical result (50) shown by the dashed lines is in good agreement with the simulation results (solid curves). The correlation times for the active particles used in model II are given by $\tau_h = 1.0$, $\tau_c = 1.0$. We set the values of the parameters to be $T_{tr} = 50$, $k = 0.5$, $k_I = 0.5$, and $k_0 = 1.0$. Other details are provided in Appendix B. For the ease of numerical simulations, the tracer is considered to be harmonically coupled to only one hot and one cold particle.

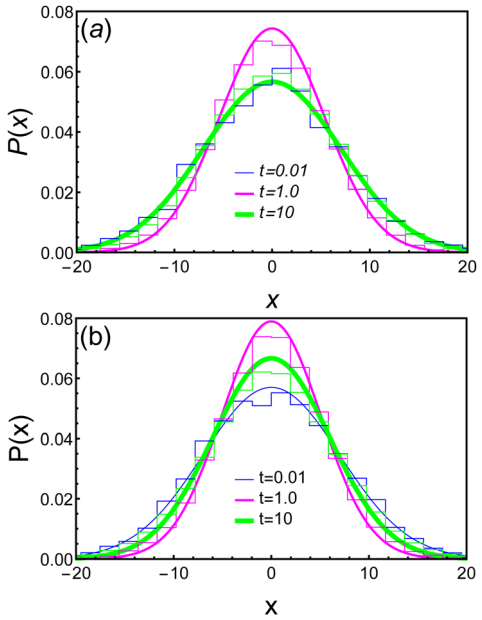

Fig. 3 PDF plotted against the displacement of the trapped tracer at different timescales for (a) model I and (b) model (II). Simulation results represented by histograms are, within numerical errors, in good agreement with the analytical expression (48). The temperatures of the hot, cold and tracer particle are $T_h = 60$, $T_c = 40$, $T_{tr} = 50$, respectively. In model (II) the correlation times for the active particles are set to $\tau_h = \tau_c = 10$. Here we consider that the tracer particle is coupled to one hot and one cold particle. Other parameters used here are given in Appendix B.

limit, the MSD in model II can be written as (see Appendix A)

$$\lim_{t\to\infty}\langle x^2(t)\rangle = D_{tr}\frac{\alpha_2+k_0^2}{\alpha_1\alpha_2}+\frac{2N_hD_hk_I^2(1+\alpha_1\tau_h)}{2\alpha_1\alpha_2(\tau_h(\alpha_1+\alpha_2\tau_h)+1)} + \frac{2N_cD_ck_I^2(1+\alpha_1\tau_c)}{2\alpha_1\alpha_2(\tau_c(\alpha_1+\alpha_2\tau_c)+1)}, \tag{6}$$

where α_1 and α_2 depend on the coupling constants k_0, k_I, and k, as well as the number N of active particles, see eqn (27c). In terms of temperatures, the MSD can be rewritten as

$$\begin{aligned}\frac{T_{eff}}{\lambda} &= \lim_{t\to\infty}\langle x^2(t)\rangle \\ &= \frac{T_{tr}}{\lambda}\frac{[\lambda\gamma_b+\lambda_0\gamma_{tr}]}{[\lambda_0\gamma_{tr}+(\lambda+N\lambda_0)\gamma_b]} \\ &+\frac{N_hT_h}{\lambda}\frac{[\gamma_I\gamma_b+(\lambda+N\lambda_0)\gamma_b\tau_h+\lambda_0\gamma_{tr}\tau_h]}{[\lambda_0\gamma_{tr}+(\lambda+N\lambda_0)\gamma_b]} \\ &\times\frac{\lambda_0\gamma_b}{[\gamma_I\gamma_b+(\lambda+N\lambda_0)\gamma_b\tau_h+\lambda_0\gamma_{tr}\tau_h+\lambda\lambda_0\tau_h^2]} \\ &+\frac{N_cT_c}{\lambda}\frac{\lambda_0\gamma_b}{[\lambda_0\gamma_{tr}+(\lambda+N\lambda_0)\gamma_b]} \\ &\times\frac{[\gamma_I\gamma_b+(\lambda+N\lambda_0)\gamma_b\tau_c+\lambda_0\gamma_{tr}\tau_c]}{[\gamma_I\gamma_b+(\lambda+N\lambda_0)\gamma_b\tau_c+\lambda_0\gamma_{tr}\tau_c+\lambda\lambda_0\tau_c^2]}.\end{aligned} \tag{7}$$

Note that even for $T_h = T_c = T_{tr}$, the effective temperature T_{eff} is not equal to T_{tr} as, by construction, the active particles are in a non-equilibrium state, and thus they keep the tracer away from equilibrium. At $\tau_h \to 0$ and $\tau_c \to 0$, the active noise reduces to the white Gaussian noise, and we recover model I, for which [see eqn (50)]

$$\begin{aligned}\lim_{t\to\infty}\langle x^2(t)\rangle &= 2\lim_{t\to\infty}\xi^2(t) \\ &= \frac{[D_hN_h+D_cN_c]k_I^2}{\alpha_1\alpha_2}+\frac{D_{tr}[\alpha_2+k_0^2]}{\alpha_1\alpha_2}.\end{aligned} \tag{8}$$

In terms of temperatures,

$$\frac{T_{eff}}{\lambda} = \lim_{t\to\infty}\langle x^2(t)\rangle = \frac{T_{tr}}{\lambda}\frac{[\lambda\gamma_b+\lambda_0\gamma_{tr}]}{[\lambda_0\gamma_{tr}+(\lambda+N\lambda_0)\gamma_b]} + \frac{\lambda_0\gamma_b}{\lambda}\frac{[N_hT_h+N_cT_c]}{[\lambda_0\gamma_{tr}+(\lambda+N\lambda_0)\gamma_b]}. \tag{9}$$

Note that unlike model II, when $T_h = T_c = T_{tr}$, we have $T_{eff} = T_{tr}$, indicating that that the particle attains equilibrium, as illustrated in Fig. 2. Furthermore, under the condition $N_hT_h + N_cT_c = (N_h + N_c)T_{tr}$, we also find $T_{eff} = T_{tr}$. Thus, the width of the distribution at shorter and longer times is the same, as reflected in panel (a) of Fig. 3. However, if $T_h > T_{tr}$ (or $T_c < T_{tr}$) keeping $T_c = T_{tr}$ (or $T_h = T_{tr}$), an additional energy is supplied to the tracer (or active particles), and as a result, the MSD is increased (or decreased) compared to the initial value, *i.e.*, $T_{eff} > T_{tr}$ (or $T_{eff} < T_{tr}$). We will discuss the energetics of the system in more detail in the next section.

To get more insight about the dynamics, the MSD $\langle x(t)^2\rangle$ is plotted in Fig. 4 for different coupling strengths k_I

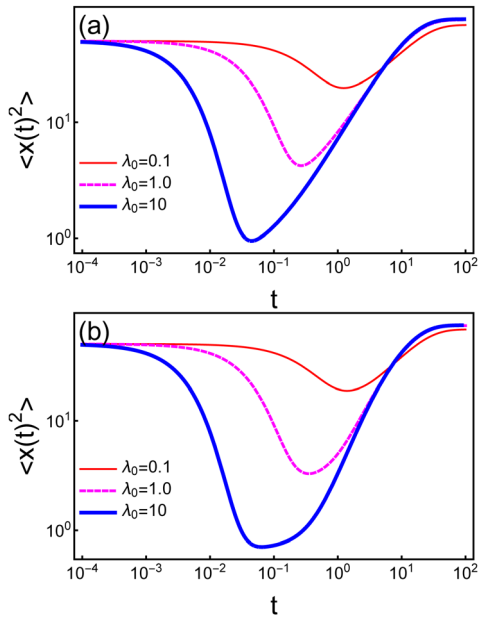

Fig. 4 Double logarithmic plot of the second central moment of the displacement given by eqn (50) *versus* time for (a) model I and (b) model II at different coupling strengths between the tracer and the active particles. The correlation times for the active particles used in model II are τ_h = 1.0, τ_c = 1.0. The number of hot and cold particles coupled to the tracer are N_h = N_c = 10. The tracer, hot and cold particles are connected to three thermostats at temperatures T_{tr} = 50, T_h = 150 and T_c = 10, respectively. Other parameters are the same as in Fig. 2.

(or equivalently, λ_0). At the crossover time t^*, the value of $\langle x(t)^2\rangle$ reaches a minimum which shifts towards shorter t^* for higher k_I values. This is true for both models, but in the case of model II, a plateau-like behaviour after t^* occurs for a longer period of time before it approaches towards the steady state. This could be due to the existence of a longer persistence time in model II. It is worth noting that the dynamical properties corresponding to model III are similar to those in model II.

4 Linear response and fluctuation–dissipation theorem

An important quantity to study in the behaviour of a non-equilibrium system is the response function $\chi(t)$ which encodes the response of the system when subjected to an external perturbation. Ignoring higher-order terms corresponding to a nonlinear response in the presence of small external force $f_{ext}(t)$, the response function in the linear regime can be defined in terms of the change in position due to the application of an external force for all possible realisations of the motion, as

$$\langle \delta x(t)\rangle = \langle x(t)\rangle_f - \langle x(t)\rangle_0 = \int_0^t dt_1 [k_0\psi(t-t_1) + \phi(t-t_1)] f_{ext}(t_1). \tag{10}$$

Eqn (32) shows how the random force $\eta(t)$ can be replaced by the external force $f_{ext}(t)$ as both forces are related to $x(t)$, in the same way, although their statistical properties are different.

From eqn (10) the response function, denoted as $\chi(t)$, can thus be computed as

$$\chi(t) = \frac{\delta\langle \delta x(t)\rangle}{\delta f_{ext}} = \Theta(t)[k_0\psi(t) + \phi(t)], \tag{11}$$

which is plotted in Fig. 5(a) for different coupling strengths k_I (or equivalently λ_0). Here $\Theta(t)$ denotes the Heaviside step function which takes care of the causality. Note that $\chi(t)$ captures, in a way, the relaxation dynamics of the system, and so it is independent of the bath models. Without coupling to the active particles, $\chi(t) = \Theta(t)e^{-kt}$, which corresponds to the response function for a tracer trapped in a harmonic potential of strength k. Fig. 5(a) shows that the response function $\chi(t)$ follows a bi-exponential decay in time, *viz.*,

$$\chi(t) = \Theta(t)\chi_s \exp\left(-\frac{t}{t_s}\right) + \Theta(t)\chi_l \exp\left(-\frac{t}{t_l}\right), \tag{12}$$

where

$$t_s = \frac{2}{\alpha_1 + \sqrt{\alpha_1^2 - 4\alpha_2}}, \tag{13a}$$

$$t_l = \frac{2}{\alpha_1 - \sqrt{\alpha_1^2 - 4\alpha_2}}, \tag{13b}$$

$$\chi_s = \frac{1}{2} + \frac{Nk_I + k - k_0}{2\sqrt{\alpha_1^2 - 4\alpha_2}}, \tag{13c}$$

$$\chi_l = \frac{1}{2} - \frac{Nk_I + k - k_0}{2\sqrt{\alpha_1^2 - 4\alpha_2}}. \tag{13d}$$

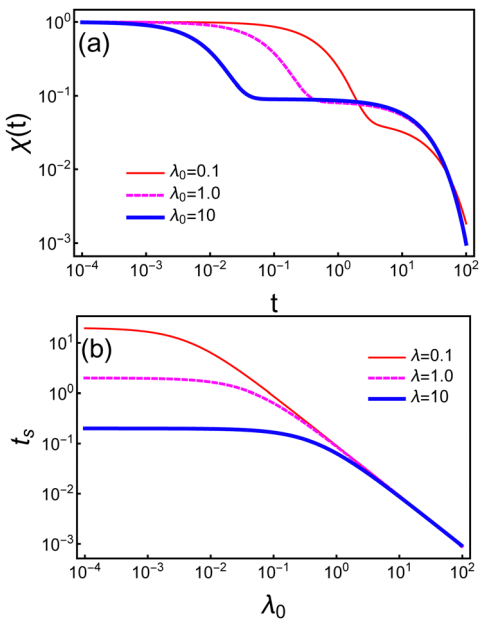

Fig. 5 (a) Double logarithmic plot of the response function (eqn (11)) as a function of time at different coupling strengths between the tracer and the active particles, keeping the strength of the harmonic potential fixed at λ = 1.0. (b) Log–log plot of t_s (see eqn (13a)) *versus* coupling strength λ_0 for different values of λ. Other parameters are the same as in Fig. 4.

So the decay is governed by two distinct functions with corresponding timescales, t_s and t_l, representing the behaviour in the two opposite time limits. The initial temporal regime, during which $\chi(t)$ exhibits a "shoulder", is dictated by the timescale t_s, while t_l corresponds to the timescale for the following regime. At the initial stage, the response function can be approximated as $\chi(t) \sim 1 - (k + Nk_I)t$, suggesting its strong dependence on the coupling strength λ_0, and it decays faster for higher values of λ_0, as shown in Fig. 5. In fact, t_s decreases monotonically with λ_0 for any finite values of λ, as shown in panel (b) of Fig. 5, and it scales as $t_s \propto \lambda_0^{-1}$ in the limit $\lambda_0 \gg \lambda$. Similar characteristics are reflected in the plots of $\langle x(t)^2 \rangle$, Fig. 4. Comparing Fig. 4 and 5, it can be concluded that the crossover time t^* also dictates the timescale which distinguishes two decay laws. At longer times, $\chi(t) \sim e^{-\frac{\alpha_2}{\alpha_1}t}$, *i.e.*, it decays exponentially which is barely affected by the coupling strength k_I, as can also be seen in Fig. 5(a).

For a system in equilibrium, the power spectrum of x (or Fourier transform of the positional autocorrelation function) is linked to the Fourier transform of the response function *via* the FDT. However, a system driven away from equilibrium violates the usual FDT with respect to the ambient temperature, but its departure from equilibrium can be quantified by introducing the concept of an effective temperature T_{eff} (or effective diffusivity D_{eff}), and thereby redefining the FDT in the Fourier space,[22,98]

$$\text{Im}[\tilde{\chi}(\omega)] = \frac{\omega}{2D_{\text{eff}}(\omega)}\text{Re}\left[\tilde{\mathbb{S}}_{xx}(\omega)\right], \tag{14}$$

where $D_{\text{eff}}(\omega)$ represents a frequency-dependent effective diffusivity. Instead of an effective temperature, one can alternatively use the term effective energy defined as $E_{\text{eff}} = k_B T_{\text{eff}}$. From (58) the imaginary part of the response function in Fourier space can be rewritten as

$$\text{Im}[\tilde{\chi}(\omega)] = \frac{\omega\left(k_0^2 + \omega^2 + Nk_0k_I\right)}{(\omega^2 - kk_0)^2 + \omega^2(k_0 + k + Nk_I)^2}. \tag{15}$$

The PSD of x depends on a chosen model of active particles, and thus it is different for each model as given by eqn (59)–(61). But all models can be mapped into each other by taking specific values of τ_h and τ_c, as discussed before. For model II, the PSD can be expressed as

$$\tilde{\mathbb{S}}_{xx}(\omega) = 2\frac{k_I^2\frac{N_hD_h}{1+\omega^2\tau_h^2} + k_I^2\frac{N_cD_c}{1+\omega^2\tau_c^2} + \left(k_0^2 + \omega^2\right)D_{\text{tr}}}{(\omega^2 - kk_0)^2 + \omega^2(k_0 + k + Nk_I)^2}, \tag{16}$$

and its plot as a function of frequency ω is shown in Fig. 6.

In the limit $\omega \to 0$ the PSD can be approximated as

$$\tilde{\mathbb{S}}_{xx}(\omega) \approx 2\frac{k_I^2\frac{N_hD_h}{1+\omega^2\tau_h^2} + k_I^2\frac{N_cD_c}{1+\omega^2\tau_c^2} + k_0^2D_{\text{tr}}}{\omega^2[k^2 + k_0^2 + N^2k_I^2 + 2(k_0 + k)Nk_I] + k^2k_0^2}, \tag{17}$$

which strongly depends on the strengths of the active forces, and therefore the spectra with different activities are separated

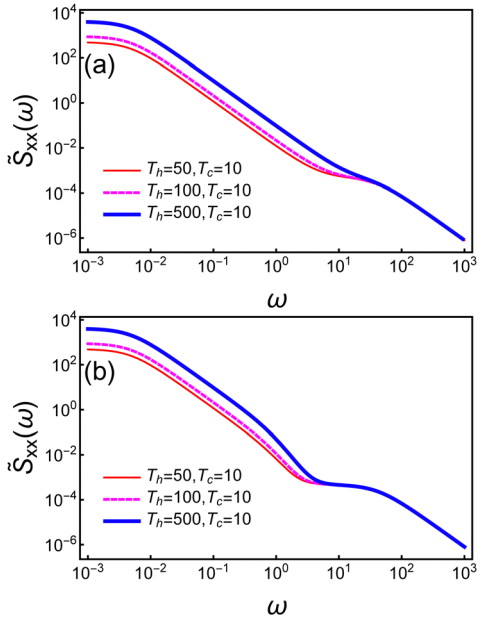

Fig. 6 Log–log plot of the power spectral density of x *versus* frequency ω for (a) model I and (b) model II with $\tau_h = \tau_c = 1$. The parameters are $N_h = N_c = 100$ and $T_{\text{tr}} = 50$. The other parameters are given by $\gamma_{\text{tr}} = 5$, $\gamma_b = 1$, $\lambda = 1$, $\lambda_0 = 1$.

at low frequencies, as shown in Fig. 6. At a higher activity, the tracer experiences larger active fluctuations, thus showing a higher spectral value. Note that such a behaviour was reported earlier in several experimental observations.[1,10,45,60] At intermediate frequencies, a significant plateau is observed for the tracer connected to AOU particles due to the presence of the persistence time, as shown in panel (b) of Fig. 6. At high frequencies,

$$\tilde{\mathbb{S}}_{xx}(\omega) \approx \frac{2D_{\text{tr}}}{\omega^2 + [k^2 + k_0^2 + N^2k_I^2 + 2(k_0 + k)Nk_I]}, \tag{18}$$

which is of typical Lorentzian form and corresponds to the thermal noise. Thus, the spectra for various activities converge to a single curve at $\omega \to \infty$. Note that eqn (18) is a generic form that appears in the expression of the PSD for various processes, including the OU process,[99,100] Brownian motion subjected to resetting,[101] and free diffusion of an active Brownian particle.[102]

Let us first consider the model I for the active particles. For this case, using eqn (60) and substituting eqn (15) in eqn (14), one can find the effective diffusivity in Fourier space as

$$\begin{aligned} D_{\text{eff}}(\omega) &= \frac{k_I^2(N_hD_h + N_cD_c)}{k_0^2 + \omega^2 + Nk_0k_I} + \frac{D_{\text{tr}}(k_0^2 + \omega^2)}{k_0^2 + \omega^2 + Nk_0k_I} \\ &= D_{\text{tr}} + \frac{k_I^2(N_hD_h + N_cD_c) - D_{\text{tr}}Nk_0k_I}{k_0^2 + \omega^2 + Nk_0k_I}, \end{aligned} \tag{19}$$

or in a similar way, the frequency-dependent effective temperature is

$$T_{\rm eff}(\omega) = \gamma_{\rm tr} D_{\rm eff}(\omega) = T_{\rm tr} + \frac{(N_{\rm h}T_{\rm h} + N_{\rm c}T_{\rm c}) - T_{\rm tr}N}{\frac{k_0}{k_I}\left[1 + N\frac{k_I}{k_0} + \frac{\omega^2}{k_0^2}\right]}. \quad (20)$$

Note that the effective temperature becomes identical to the temperature of the tracer (*i.e.*, $T_{\rm eff}(\omega) = T_{\rm tr}$) when $T_{\rm tr} = T_{\rm h} = T_{\rm c}$. This describes an equilibrium situation. In any other case, $T_{\rm eff}(\omega)$ differs from $T_{\rm tr}$, and thus it represents a non-equilibrium system. Note that here one can define the active energy as

$$E_{\rm act}(\omega) = k_{\rm B}[T_{\rm eff}(\omega) - T_{\rm tr}], \quad (21)$$

which measures the sole contributions of active fluctuations.[45] For model II, the frequency-dependent effective temperature can be calculated using eqn (15), (59) and (14),

$$\begin{aligned} T_{\rm eff}(\omega) &= \gamma_{\rm tr} D_{\rm eff}(\omega) \\ &= T_{\rm tr} + \frac{\frac{N_{\rm h}T_{\rm h}}{1+\omega^2\tau_{\rm h}^2} + \frac{N_{\rm c}T_{\rm c}}{1+\omega^2\tau_{\rm c}^2} - T_{\rm tr}N}{\frac{k_0}{k_I}\left[1 + N\frac{k_I}{k_0} + \frac{\omega^2}{k_0^2}\right]}. \end{aligned} \quad (22)$$

For $T_{\rm tr} = T_{\rm h} = T_{\rm c}$, $T_{\rm eff}(\omega) \neq T_{\rm tr}$, and as mentioned earlier, this system always stays at non-equilibrium.

Fig. 7 shows the plot of $T_{\rm eff}(\omega)$ for the two models. Note that, depending on the values of $T_{\rm h}$ and $T_{\rm c}$, $T_{\rm eff}(\omega)$ becomes larger or smaller compared to $T_{\rm tr}$, and this difference of temperature is clearly visible in the (activity-dominated) low-ω regime, in sync with the PSD analysis. Interestingly, $T_{\rm eff}(\omega)$ in model II exhibits a non-monotonic variation with ω, *i.e.*, at an intermediate frequency ω^* it reaches a minimum which diminishes at vanishing persistence times. Therefore, such behaviour captures a signature of the persistent motion.

Fig. 8 illustrates how ω^* varies with persistence times ($\tau_{\rm h}$ and $\tau_{\rm c}$) and the coupling strength λ_0. Increasing persistence times causes ω^* to shift towards smaller values, while an increase in λ_0 results in higher values of ω^*. When the coupling strength is higher, the tracer's motion is quickly constrained by stronger interaction with the active particles before it relaxes towards the steady state. This implies a higher ω^* value and a significant decrease in effective energy [*cf.* Fig. 5]. On the other hand, in a highly persistent environment, the tracer interacts with the particles over longer periods, expending more energy before reaching a steady state. As a result, $E_{\rm act}(\omega)$ decreases significantly over a wider range of frequencies, and thus its minimum occurs at a lower ω^*. The result is further clarified in our subsequent analysis.

Another way of characterising the non-equilibrium activity is to calculate the energy dissipation rate. Using the Harada–Sasa equality, the spectral density of dissipation rate can be expressed as[22,98]

$$I_{\rm diss}(\omega) = \gamma_{\rm tr}\omega\left[\omega\tilde{\mathbb{S}}_{xx}(\omega) - 2D_{\rm tr}{\rm Im}[\tilde{\chi}(\omega)]\right], \quad (23)$$

and thus the integration of its spectral density over all values of ω results in the average rate of energy dissipation, *i.e.*, the energy transferred from the surroundings to the tracer. So the average dissipation rate can be written as

$$\langle J\rangle = \frac{1}{2\pi}\int_{-\infty}^{+\infty} {\rm d}\omega I_{\rm diss}(\omega). \quad (24)$$

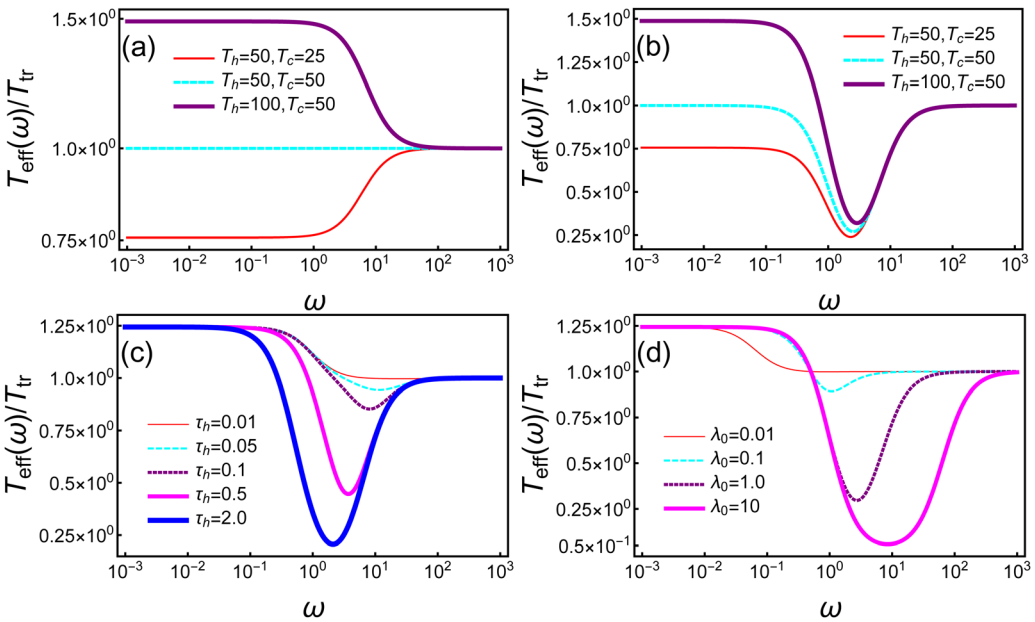

Fig. 7 Double logarithmic plot of the effective temperature in frequency domain, scaled by temperature of the tracer as function of frequency ω for (a) model I and (b) model II where $\tau_{\rm h} = \tau_{\rm c} = 1$ and $T_{\rm tr} = 50$. Other parameters are the same as in Fig. 6. In panels (c) and (d), the effective temperature for model II is plotted as a function of ω for different values of the persistence time $\tau_{\rm h}$ and the interaction strength λ_0, respectively, setting the temperatures as $T_{\rm h} = 100$, $T_{\rm c} = 25$ and $T_{\rm tr} = 50$. For panel (c), we take $\lambda_0 = 1.0$, and for panel (d), $\tau_{\rm h} = \tau_{\rm c} = 1$. Other parameters are the same as in Fig. 6.

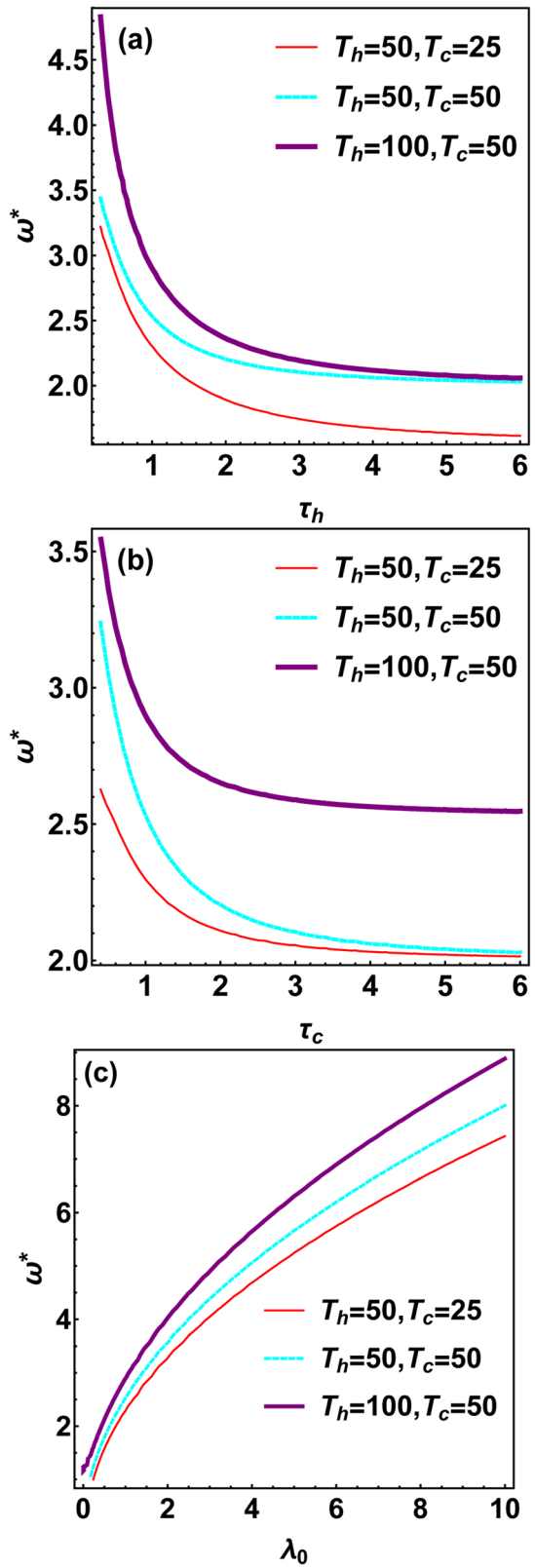

Fig. 8 Plots of ω^* for model II as functions of (a) τ_h while keeping τ_c = 1 and λ_0 = 1, (b) τ_c while keeping τ_h = 1 and λ_0 = 1, and (c) λ_0 when τ_h = τ_c = 1, with T_{tr} = 50. The curves are obtained by numerically solving the equation $\left.\frac{dT_{eff}(\omega)}{d\omega}\right|_{\omega=\omega^*} = 0$, using eqn (22). Other parameters are the same as in Fig. 6.

With the help of eqn (15) and (57), the average dissipation rate given in eqn (24) is calculated exactly for the two models. For model I, it is given by

$$\langle J\rangle = \frac{\sqrt{2}k_I k_0 k_B[-T_{tr}(N_c+N_h)+(T_cN_c+T_hN_h)]}{\sqrt{\alpha_1^2+\sqrt{\alpha_1^2-4\alpha_2}\alpha_1-2\alpha_2}+\sqrt{\alpha_1^2-\sqrt{\alpha_1^2-4\alpha_2}\alpha_1-2\alpha_2}}, \tag{25}$$

while for model II, the energy dissipation rate is

$$\begin{aligned}\langle J\rangle &= -\frac{k_0k_Ik_B}{2}\left[\frac{T_hN_h\tau_h}{(\alpha_2\tau_h^2+1)^2-\alpha_1^2\tau_h^2}+\frac{T_cN_c\tau_c}{(\alpha_2\tau_c^2+1)^2-\alpha_1^2\tau_c^2}\right.\\ &\quad+\frac{\sqrt{2}\alpha_{22}}{\alpha_{12}}\sqrt{\alpha_1^2+\sqrt{\alpha_1^2-4\alpha_2}\alpha_1-2\alpha_2}\\ &\quad\left.+\frac{\sqrt{2}\alpha_{21}}{\alpha_{11}}\sqrt{\alpha_1^2-\sqrt{\alpha_1^2-4\alpha_2}\alpha_1-2\alpha_2}\right],\end{aligned} \tag{26}$$

where the variables are given as

$$\begin{aligned}\alpha_{11} &= \alpha_1\Big(\tau_h^2\tau_c^2\alpha_1^5-\sqrt{\alpha_1^2-4\alpha_2}\tau_h^2\tau_c^2\alpha_1^4-\big((6\alpha_2\tau_c^2+1)\tau_h^2\\ &\quad+\tau_c^2\big)\alpha_1^3+\sqrt{\alpha_1^2-4\alpha_2}\big((4\alpha_2\tau_c^2+1)\tau_h^2+\tau_c^2\big)\alpha_1^2\\ &\quad+4\alpha_2\big((2\alpha_2\tau_c^2+1)\tau_h^2+\tau_c^2\big)\alpha_1-2\sqrt{\alpha_1^2-4\alpha_2}\\ &\quad\times\big(\alpha_2^2\tau_h^2\tau_c^2+\alpha_2(\tau_h^2+\tau_c^2)+1\big)\big),\end{aligned} \tag{27a}$$

$$\begin{aligned}\alpha_{21} &= -2(T_cN_c+T_hN_h)-\Big(\alpha_1\sqrt{\alpha_1^2-4\alpha_2}-\alpha_1^2+2\alpha_2\Big)\\ &\quad\times\big(T_cN_c\tau_h^2+T_hN_h\tau_c^2\big)+T_{tr}(N_c+N_h)\\ &\quad\times\Big[(\tau_c^2\alpha_1^4-\sqrt{\alpha_1^2-4\alpha_2}\tau_c^2\alpha_1^3-(4\alpha_2\tau_c^2+1)\alpha_1^2\\ &\quad+\sqrt{\alpha_1^2-4\alpha_2}\times\alpha_1(2\alpha_2\tau_c^2+1)+2\alpha_2(\alpha_2\tau_c^2+1)\Big)\tau_h^2\\ &\quad+\Big(\Big(\sqrt{\alpha_1^2-4\alpha_2}-\alpha_1\Big)\alpha_1+2\alpha_2\Big)\tau_c^2+2\Big],\end{aligned} \tag{27b}$$

$$\begin{aligned}\alpha_{12} &= \alpha_1\Big(\tau_h^2\tau_c^2\alpha_1^5+\sqrt{\alpha_1^2-4\alpha_2}\tau_h^2\tau_c^2\alpha_1^4-\big((6\alpha_2\tau_c^2+1)\tau_h^2\\ &\quad+\tau_c^2\big)\alpha_1^3\sqrt{\alpha_1^2-4\alpha_2}\big((4\alpha_2\tau_c^2+1)\tau_h^2+\tau_c^2\big)\alpha_1^2\\ &\quad+4\alpha_2\big((2\alpha_2\tau_c^2+1)\tau_h^2+\tau_c^2\big)\alpha_1+2\sqrt{\alpha_1^2-4\alpha_2}\\ &\quad\times\big(\alpha_2^2\tau_h^2\tau_c^2+\alpha_2(\tau_h^2+\tau_c^2)+1\big)\big),\end{aligned} \tag{27c}$$

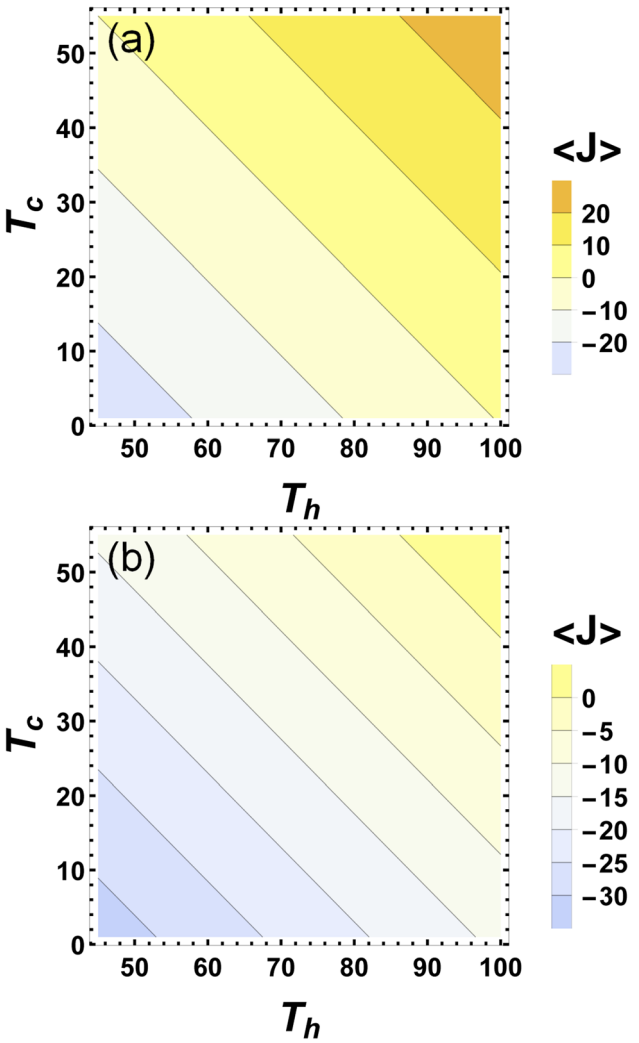

Fig. 9 Contour plot of the average dissipation rate $\langle J\rangle$ as function of the temperatures of the hot and cold particles in (a) model I and (b) model II where $\tau_h = \tau_c = 0.01$. The various coloured regions in the plot correspond to different ranges of $\langle J\rangle$ values, as indicated in the legend. The contour lines correspond to equal magnitude of $\langle J\rangle$. Other parameters are the same as in Fig. 6.

$$\begin{aligned}\alpha_{22} &= -2(T_cN_c + T_hN_h) + \left(\alpha_1\sqrt{\alpha_1^2 - 4\alpha_2} + \alpha_1^2 - 2\alpha_2\right)\\ &\times \left(T_cN_c\tau_h^2 + T_hN_h\tau_c^2\right) + T_{tr}(N_c + N_h)\left[\left(\tau_c^2\alpha_1^4\right.\right.\\ &+ \sqrt{\alpha_1^2 - 4\alpha_2}\tau_c^2\alpha_1^3 - \left(4\alpha_2\tau_c^2 + 1\right)\alpha_1^2 - \sqrt{\alpha_1^2 - 4\alpha_2}\\ &\times \left(2\alpha_2\tau_c^2 + 1\right)\alpha_1 + 2\alpha_2\left(\alpha_2\tau_c^2 + 1\right)\tau_h^2\\ &- \left.\left(\alpha_1\sqrt{\alpha_1^2 - 4\alpha_2} + \alpha_1^2 - 2\alpha_2\right)\tau_c^2 + 2\right].\end{aligned} \tag{27d}$$

Fig. 9 demonstrates the variation of the $\langle J\rangle$ values for a wide range of temperatures associated with hot and cold particles. It is evident that the rate increases with increasing T_h (or T_c) for a fixed value of T_c (or T_h). In model I, $\langle J\rangle > 0$ if the tracer is connected to all hot particles whose temperatures are greater than T_{tr}, and in the opposite case when all connected particles have temperatures lower than that of the tracer, $\langle J\rangle < 0$. The dissipation rate is exactly zero if $T_{tr} = (T_cN_c + T_hN_h)/(N_h + N_c)$.

Now consider the case when the active force is described by the OU process. Interestingly, $\langle J\rangle < 0$ even if the tracer is in contact with all hot particles, as shown in panel (b) of Fig. 10. This may seem counter-intuitive, but this behaviour has already been anticipated in panel (b) of Fig. 7. The negativity of the $\langle J\rangle$ values implies that the active particles must have a lower (effective) temperature as compared to the tracer and, as a result, a net energy is dissipated to the active particles. In fact, at the steady state (without thermal fluctuations) a single active particle can be characterised by an effective temperature (T_{act}) which is smaller than the one (T) in its equilibrium, here $T_{act,i} = T_i/(1 + k_0\tau_i)$, and $i = h$ and $i = c$ for hot and cold particles, respectively. Note that, for any non-zero values of τ_i, $T_{act,i} < T_i$. Thus with the increment of τ_i, the effective temperature of the active particle decreases, and this appears to be one of the reasons for the lowering of $\langle J\rangle$. The value of $\langle J\rangle$ will be lowered to a greater extent if it is a hot particle whose effective temperature is decreased due to longer persistence. This fact is reflected in panel (a) of Fig. 10. One can thus infer that there is a net energy flow to active particles of this kind, and, if there are a large number of active particles coupled to the tracer, $\langle J\rangle$ decreases significantly, as can be seen from panel (b) of Fig. 10. However at a fixed parametric region, there exists an optimal value of number ratio (N_h/N_c) for which $\langle J\rangle$ is maximum, and this maximum moves from a region where $N_h/N_c > 1$ to a region where $N_h/N_c < 1$, as the number of active particles increases. Note that here only the active contributions have been considered which yields negative dissipation rate. Conceptually, the dissipation rate becomes positive, *i.e.*, a net energy is supplied to the tracer while coupled to active particles if the thermal part is included in the dynamics of active particles or/and the active force is much stronger than the thermal one. However, using the above analysis of model II one can justify the surprising observation in ref. 32 where the activity is responsible for the suppression of non-equilibrium fluctuations.

For fixed values of diffusivities $D_{h,m}$ and $D_{c,m}$, model III produces the same results as model II mentioned above. However, it differs when the amplitudes of the active force are held fixed. The results for this case are shown in Fig. 11. In contrast to model II, the dissipation rate $\langle J\rangle$ varies non-monotonically with respect to the persistence times, as shown in panel (a) of Fig. 11. At an intermediate region in the parametric space of $\{\tau_h,\tau_c\}$, $\langle J\rangle$ is at its maximum. Relying on a similar argument as presented for model II, the behaviour at small persistence times could be attributed to its dependence on the effective temperature which is given by $T_{act,i} = \dfrac{\gamma_b G_i\tau_i}{1 + k_0\tau_i}$, where $i = \{h,c\}$ for hot and cold particles, respectively. Note that with an increase in the persistence time, the effective temperature also increases and reaches a fixed value, but the correlation of the active force decays exponentially in time with a correlation timescale given by τ_i. The variation of $\langle J\rangle$ with respect to

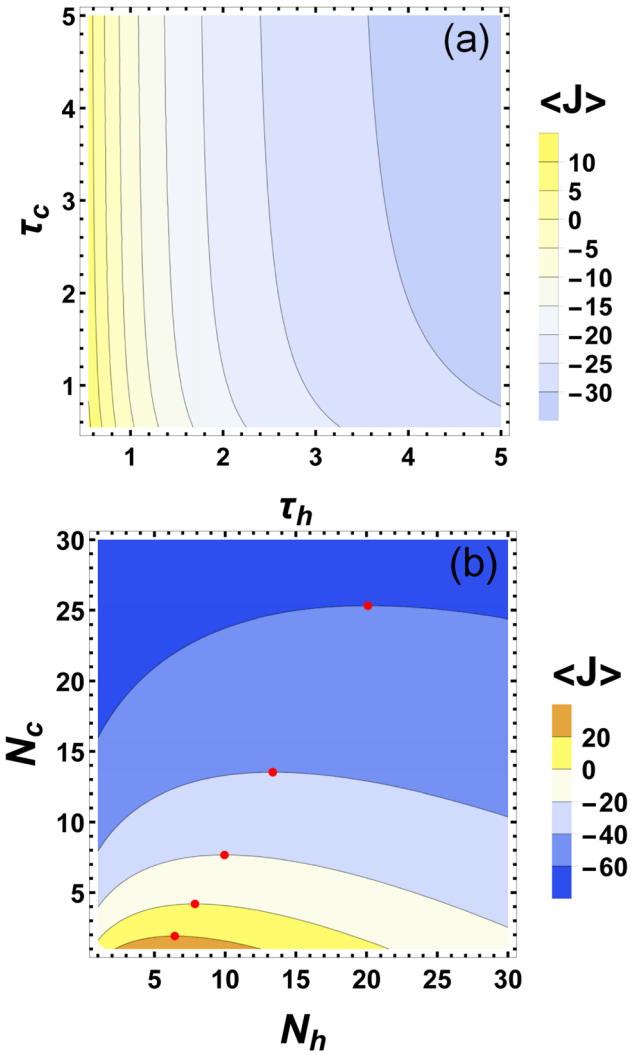

Fig. 10 Model II: active particles driven by coloured Gaussian noises. Contour plot of (a) the average dissipation rate $\langle J \rangle$ as function of persistence times where $N_h = N_c = 2$, and (b) the numbers of hot and cold particles where $\tau_h = \tau_c = 0.65$. Each red dot in panel (b) indicates the point at which N_c is maximum for the respective contour. Here the temperatures of the particles are taken as $T_h = 500$, $T_c = 50$ and $T_{tr} = 100$. Other parameters are given as $\gamma_{tr} = 5$, $\gamma_b = 1$, $\lambda = 1$, $\lambda_0 = 1$.

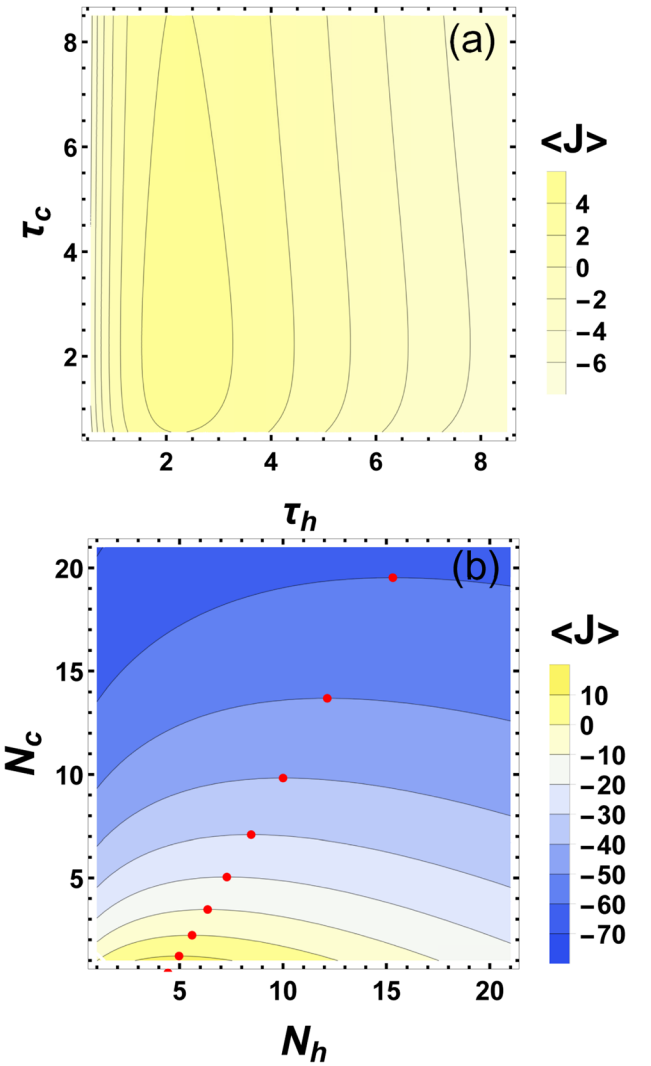

Fig. 11 Model III: active particles governed by MOU processes. Contour plot of (a) the average dissipation rate $\langle J \rangle$ as function of persistence times where $N_h = N_c = 2$, and (b) the numbers of hot and cold particles where $\tau_h = \tau_c = 0.65$. In panel (b), each red dot on the respective contour indicates the point at which N_c has maximum value. Here, the amplitudes of the active forces are considered as constants, and their values are given as $G_h = 600$ and $G_c = 50$. Other parameters are given as $T_{tr} = 100$, $\gamma_{tr} = 5$, $\gamma_b = 1$, $\lambda = 1$, $\lambda_0 = 1$.

the number ratio follows a similar trend as model II, as shown in panel (b) of Fig. 11. Model III is suitable for characterising the bath where the motion of active particles is induced by self-propulsion with a fixed average speed, such as in a bacterial bath.[17]

5 Conclusions

Here we developed an analytical tool to generalise the common model for the dynamics of a tracer in a non-equilibrium bath. With this technique, we obtained exact time-dependent solutions of important dynamical observables for the model of bath particles driven by any kind of Gaussian noise. Some important results we obtained in the present study are given as follows. For the effective motion of the tracer, the MSD of its positional distribution changes non-monotonically with time, and it reaches a steady state at a long time characterised by an effective temperature (T_{eff}), dictating its departure from equilibrium. T_{eff} for model I [see eqn (9)] closely resembles the one reported in ref. 63. We also present the results for T_{eff} when the dynamics of bath particles are governed by the OU processes.

The active contributions are encoded in the low-frequency regime of the PSD, where enhanced fluctuations occur, as observed experimentally; *e.g.*, see ref. 10 and 45. In model II and III, the persistent nature is highlighted in the plateau region of the PSD plot. The response function obeys double-exponential decay laws, with two distinct timescales that

strongly depend on the interaction strength between the tracer and the bath particles. In a viscoelastic bath, the existence of two timescales was reported earlier in the hopping dynamics of a tracer crossing the barrier.[103]

A higher effective temperature, associated with increased activity, results in a higher dissipation rate, allowing for an estimation of non-equilibrium fluctuations, as discussed in ref. 10, 45 and 47. However, we show that for the case where the temperature of the active particles is lower or the active particles undergo OU dynamics, non-equilibrium fluctuations are significantly reduced, in agreement with the findings in ref. 63. More specifically, longer persistence leads to a more substantial reduction of non-equilibrium fluctuations.

Extensions of our present study are quite straightforward to incorporate, *e.g.*, in terms of alternative models of the active force such as a Poisson noise when the dynamical description goes beyond the Gaussian approximation. It can also be applied to study other thermodynamic quantities such as heat, work and entropy production. Finally, we note that it will be interesting to employ a similar approach to explore how a tracer behaves in an active medium, considering scenarios where the interaction potential between the tracer and bath particles is anharmonic, when the particles within the medium interact with each other, or when the medium itself is an active polymeric network.

Abbreviations and symbols

AOU	Active Ornstein–Uhlenbeck
FDT	Fluctuation–dissipation theorem
MOU	Modified active Ornstein–Uhlenbeck
MSD	Mean squared displacement
OU	Ornstein–Uhlenbeck
PDF	Probability density function
PSD	Power spectral density

Conflicts of interest

There are no conflicts of interest to declare.

Appendix

A Derivation of the PDF

The solution of eqn (1b) and (1c) can be expressed as

$$x_j(t) = x_j(0)\mathrm{e}^{-k_0 t} + k_0\int_0^t \mathrm{d}t_1 \mathrm{e}^{-k_0(t-t_1)}x(t_1) + \int_0^t \mathrm{d}t_1 \mathrm{e}^{-k_0(t-t_1)}\eta_j(t_1). \tag{28}$$

Using the above, eqn (1a) can be recast as

$$\begin{aligned}\dot{x}(t) \;=\; & -(k+Nk_I)x(t) + Nk_0k_I\int_0^t \mathrm{d}t_1 \mathrm{e}^{-k_0(t-t_1)}x(t_1) \\ & + k_I\sum_{i=1}^{N_\mathrm{h}} x_{\mathrm{h},i}(0)\mathrm{e}^{-k_0 t} \\ & + k_I\sum_{i=1}^{N_\mathrm{c}} x_{\mathrm{c},i}(0)\mathrm{e}^{-k_0 t} + k_I\sum_{i=1}^{N_\mathrm{h}}\int_0^t \mathrm{d}t_1 \mathrm{e}^{-k_0(t-t_1)}\eta_{\mathrm{h},i}(t_1) \\ & + k_I\sum_{i=1}^{N_\mathrm{c}}\int_0^t \mathrm{d}t_1 \mathrm{e}^{-k_0(t-t_1)}\eta_{\mathrm{c},i}(t_1) + \eta(t),\end{aligned} \tag{29}$$

where $N = N_\mathrm{h} + N_\mathrm{c}$. Upon Laplace transform of eqn (29) one obtains

$$\begin{aligned}s\tilde{x}(s) - x(0) \;=\; & -(k+Nk_I)\tilde{x}(s) + Nk_0k_I\frac{\tilde{x}(s)}{s+k_0} + k_I\sum_{i=1}^{N_\mathrm{h}}\frac{x_{\mathrm{h},i}(0)}{s+k_0} \\ & + k_I\sum_{i=1}^{N_\mathrm{c}}\frac{x_{\mathrm{c},i}(0)}{s+k_0} + k_I\sum_{i=1}^{N_\mathrm{h}}\frac{\tilde{\eta}_{\mathrm{h},i}(s)}{s+k_0} + k_I\sum_{i=1}^{N_\mathrm{c}}\frac{\tilde{\eta}_{\mathrm{c},i}(s)}{s+k_0} + \tilde{\eta}(s).\end{aligned} \tag{30}$$

After rearranging the terms of the above, the solution in the Laplace domain can be expressed as

$$\begin{aligned}\tilde{x}(s) \;=\; & x(0)\frac{s+k_0}{s^2+(k_0+Nk_I+k)s+kk_0} \\ & + \tilde{\eta}(s)\frac{s+k_0}{s^2+(k_0+Nk_I+k)s+kk_0} \\ & + k_I\sum_{i=1}^{N_\mathrm{h}}\frac{x_{\mathrm{h},i}(0)}{s^2+(k_0+Nk_I+k)s+kk_0} \\ & + k_I\sum_{i=1}^{N_\mathrm{c}}\frac{x_{\mathrm{c},i}(0)}{s^2+(k_0+Nk_I+k)s+kk_0} \\ & + k_I\sum_{i=1}^{N_\mathrm{h}}\frac{\tilde{\eta}_{\mathrm{h},i}(s)}{s^2+(k_0+Nk_I+k)s+kk_0} \\ & + k_I\sum_{i=1}^{N_\mathrm{c}}\frac{\tilde{\eta}_{\mathrm{c},i}(s)}{s^2+(k_0+Nk_I+k)s+kk_0}.\end{aligned} \tag{31}$$

Now one can perform the inverse Laplace transform of eqn (31), yielding

$$\begin{aligned}x(t) \;=\; & x(0)[k_0\psi(t)+\phi(t)] + k_I\psi(t)\left[\sum_{i=1}^{N_\mathrm{h}} x_{\mathrm{h},i}(0) + \sum_{i=1}^{N_\mathrm{c}} x_{\mathrm{c},i}(0)\right] \\ & + k_I\sum_{i=1}^{N_\mathrm{h}}\int_0^t \mathrm{d}t_1\psi(t-t_1)\eta_{\mathrm{h},i}(t_1) + k_I\sum_{i=1}^{N_\mathrm{c}}\int_0^t \mathrm{d}t_1\psi(t-t_1)\eta_{\mathrm{c},i}(t_1) \\ & + \int_0^t \mathrm{d}t_1[k_0\psi(t-t_1)+\phi(t-t_1)]\eta(t_1),\end{aligned} \tag{32}$$

where

$$\phi(t) = \mathrm{e}^{-\frac{\alpha_1 t}{2}}\cosh\left(\frac{t}{2}\sqrt{{\alpha_1}^2-4\alpha_2}\right) - \frac{\alpha_1 \mathrm{e}^{-\frac{\alpha_1 t}{2}}\sinh\left(\frac{t}{2}\sqrt{{\alpha_1}^2-4\alpha_2}\right)}{\sqrt{{\alpha_1}^2-4\alpha_2}}, \tag{33}$$

$$\psi(t) = \frac{2\mathrm{e}^{-\frac{\alpha_1 t}{2}}\sinh\left(\frac{t}{2}\sqrt{{\alpha_1}^2-4\alpha_2}\right)}{\sqrt{{\alpha_1}^2-4\alpha_2}}, \tag{34}$$

$$\alpha_1 = k_0 + Nk_I + k, \tag{35}$$

and

$$\alpha_2 = kk_0. \tag{36}$$

By virtue of eqn (43), the PDF can be expressed as[91,104]

$$\begin{aligned} P(x,t) &= \langle\delta(x-x(t))\rangle = \frac{1}{2\pi}\int \mathrm{d}q \mathrm{e}^{-iqx}\langle \mathrm{e}^{iqx(t)}\rangle_{x(t)} \\ &= \frac{1}{2\pi}\int \mathrm{d}q \mathrm{e}^{-iqx}\langle \mathrm{e}^{iqx(0)[k_0\psi(t)+\phi(t)]}\rangle_{x(0)} \\ &\quad\times \prod_{i=1}^{N_\mathrm{h}}\langle \mathrm{e}^{iqk_I\psi(t)x_{\mathrm{h},i}(0)}\rangle_{x(0),x_{\mathrm{h},i}(0),x_{\mathrm{c},i}(0)} \\ &\quad\times \prod_{i=1}^{N_\mathrm{c}}\langle \mathrm{e}^{iqk_I\psi(t)x_{\mathrm{c},i}(0)}\rangle_{x(0),x_{\mathrm{h},i}(0),x_{\mathrm{c},i}(0)} \\ &\quad\times \prod_{i=1}^{N_\mathrm{h}}\langle \mathrm{e}^{iqk_I\int_0^t \mathrm{d}t_1\psi(t-t_1)\eta_{\mathrm{h},i}(t_1)}\rangle_{\eta_{\mathrm{h},i}(t_1)} \\ &\quad\times \prod_{i=1}^{N_\mathrm{c}}\langle \mathrm{e}^{iqk_I\int_0^t \mathrm{d}t_1\psi(t-t_1)\eta_{\mathrm{c},i}(t_1)}\rangle_{\eta_{\mathrm{c},i}(t_1)} \\ &\quad\times \langle \mathrm{e}^{iq\int_0^t \mathrm{d}t_1[k_0\psi(t-t_1)+\phi(t-t_1)]\eta(t_1)}\rangle_{\eta(t_1)}, \end{aligned} \tag{37}$$

where $\langle\cdots\rangle_{y(t)}$ represents the ensemble average over all realisations of variable $y(t)$. As a simple assumption, one can consider that all the particles are decoupled to the tracer at time $t = 0$, and the tracer is just confined in the potential $V(x_0) = \frac{1}{2}kx_0^2$ (initial condition I). So the PDF in eqn (37) can be written as

$$\begin{aligned} P(x,t) &= \frac{1}{2\pi}\sqrt{\frac{k}{2\pi D_\mathrm{tr}}}\int \mathrm{d}q \mathrm{e}^{-iqx}\prod_{i=1}^{N_\mathrm{h}}\prod_{j=1}^{N_\mathrm{c}}\int \mathrm{d}x(0)\mathrm{e}^{iqx(0)[k_0\psi(t)+\phi(t)]-\frac{k}{2D_\mathrm{tr}}x(0)^2} \\ &\quad\times \left\langle \mathrm{e}^{iq\int_0^t \mathrm{d}t_1[k_0\psi(t-t_1)+\phi(t-t_1)]\eta(t_1)}\right\rangle_{\eta(t_1)} \\ &\quad\times \left\langle \mathrm{e}^{iqk_I\int_0^t \mathrm{d}t_1\psi(t-t_1)\eta_{\mathrm{h},i}(t_1)}\right\rangle_{\eta_{\mathrm{h},i}(t_1)} \\ &\quad\times \left\langle \mathrm{e}^{iqk_I\int_0^t \mathrm{d}t_1\psi(t-t_1)\eta_{\mathrm{c},i}(t_1)}\right\rangle_{\eta_{\mathrm{c},i}(t_1)} \\ &= \frac{1}{2\pi}\int \mathrm{d}q \mathrm{e}^{-iqx}\mathrm{e}^{-D_\mathrm{tr}q^2\int_0^t \mathrm{d}t_1[k_0\psi(t-t_1)+\phi(t-t_1)]^2-\xi_1^2(t)q^2} \\ &\quad\times \left\langle \mathrm{e}^{iqk_I\int_0^t \mathrm{d}t_1\psi(t-t_1)\eta_{\mathrm{h},i}(t_1)}\right\rangle_{\eta_{\mathrm{h},i}(t_1)} \\ &\quad\times \left\langle \mathrm{e}^{iqk_I\int_0^t \mathrm{d}t_1\psi(t-t_1)\eta_{\mathrm{c},i}(t_1)}\right\rangle_{\eta_{\mathrm{c},i}(t_1)}, \end{aligned} \tag{38}$$

where

$$\xi_1^2(t) = \frac{D_\mathrm{tr}}{2k}[k_0\psi(t)+\phi(t)]^2. \tag{39}$$

One can also assume another initial condition which states that the active particles evolve from steady states having densities of the form: $P(x_i(0)) \propto \mathrm{e}^{-\frac{k_0}{2D_\mathrm{eff}}x_i(0)^2}$, with D_eff being the effective diffusivity (initial condition II). Using those initial (normalised) densities, one can write the average over x_0, $x_\mathrm{h}(0)$ and $x_\mathrm{c}(0)$ explicitly, and thereafter integrating over these variables in eqn (48), one obtains

$$\begin{aligned} &P(x,t) \\ &= \frac{1}{2\pi}\int \mathrm{d}q \mathrm{e}^{-iqx}\sqrt{\frac{k}{2\pi D_\mathrm{tr}}}\sqrt{\frac{N_\mathrm{h}N_\mathrm{c}}{4\pi^2}\left(\frac{k_I}{D_\mathrm{tr}}+\frac{k_0}{D_{\mathrm{h,eff}}}\right)\left(\frac{k_I}{D_\mathrm{tr}}+\frac{k_0}{D_{\mathrm{c,eff}}}\right)} \\ &\quad\times \prod_{i=1}^{N_\mathrm{h}}\prod_{j=1}^{N_\mathrm{c}}\int \mathrm{d}x(0)\int \mathrm{d}x_{\mathrm{h},i}(0)\int \mathrm{d}x_{\mathrm{c},j}(0)\mathrm{e}^{iqx(0)[k_0\psi(t)+\phi(t)]+iqk_I\psi(t)x_{\mathrm{h},i}(0)} \\ &\quad\times \mathrm{e}^{iqk_I\psi(t)x_{\mathrm{c},j}(0)}\mathrm{e}^{-\frac{k}{2D_\mathrm{tr}}x(0)^2-\frac{k_I}{2D_\mathrm{tr}}\left(x(0)-x_{\mathrm{h},i}(0)\right)^2-\frac{k_I}{2D_\mathrm{tr}}\left(x(0)-x_{\mathrm{c},j}(0)\right)^2} \\ &\quad\times \mathrm{e}^{-\frac{k_0}{2D_{\mathrm{h,eff}}}\left(x_{\mathrm{h},i}(0)-x(0)\right)^2-\frac{k_0}{2D_{\mathrm{c,eff}}}\left(x_{\mathrm{c},j}(0)-x(0)\right)^2} \\ &\quad\times \left\langle \mathrm{e}^{iqk_I\int_0^t \mathrm{d}t_1\psi(t-t_1)\eta_{\mathrm{h},i}(t_1)}\right\rangle_{\eta_{\mathrm{h},i}(t_1)} \\ &\quad\times \left\langle \mathrm{e}^{iqk_I\int_0^t \mathrm{d}t_1\psi(t-t_1)\eta_{\mathrm{c},i}(t_1)}\right\rangle_{\eta_{\mathrm{c},i}(t_1)}\left\langle \mathrm{e}^{iq\int_0^t \mathrm{d}t_1[k_0\psi(t-t_1)+\phi(t-t_1)]\eta(t_1)}\right\rangle_{\eta(t_1)} \\ &= \frac{1}{2\pi}\int \mathrm{d}q \mathrm{e}^{-iqx}\mathrm{e}^{-D_\mathrm{tr}q^2\int_0^t \mathrm{d}t_1[k_0\psi(t-t_1)+\phi(t-t_1)]^2-\xi_1^2(t)q^2} \\ &\quad\times \left\langle \mathrm{e}^{iqk_I\int_0^t \mathrm{d}t_1\psi(t-t_1)\eta_{\mathrm{h},i}(t_1)}\right\rangle_{\eta_{\mathrm{h},i}(t_1)} \\ &\quad\times \left\langle \mathrm{e}^{iqk_I\int_0^t \mathrm{d}t_1\psi(t-t_1)\eta_{\mathrm{c},i}(t_1)}\right\rangle_{\eta_{\mathrm{c},i}(t_1)}. \end{aligned} \tag{40}$$

Here,

$$\begin{aligned}\xi_1^2(t) =& \frac{D_{\rm tr}[k_0\psi(t)+\phi(t)][k_I N\psi(t)+k_0\psi(t)+\phi(t)]}{2k}\\ &+\frac{D_{\rm tr}k_I N_{\rm h}\psi(t)}{2k\left(D_{\rm tr}k_0+k_I D_{\rm h,eff}\right)}\\ &\times\left[D_{\rm tr}k_0^2\psi(t)+k_0\left\{D_{\rm tr}\phi(t)+k_I\psi(t)\left(D_{\rm h,eff}+D_{\rm tr}N\right)\right\}\right.\\ &\left.+k_I D_{\rm h,eff}\{k_I N\psi(t)+k\psi(t)+\phi(t)\}\right]+\frac{D_{\rm tr}k_I N_{\rm c}\psi(t)}{2k\left(D_{\rm tr}k_0+k_I D_{\rm c,eff}\right)}\\ &\times\left[k_0\left\{D_{\rm tr}\phi(t)+k_I\psi(t)\left(D_{\rm c,eff}+D_{\rm tr}N\right)\right\}\right.\\ &\left.+k_I D_{\rm c,eff}\{k_I N\psi(t)+k\psi(t)+\phi(t)\}+D_{\rm tr}k_0^2\psi(t)\right],\end{aligned} \tag{41}$$

which becomes identical to eqn (50) if one takes $k_I = 0$ in eqn (52). For a Gaussian noise $\eta(t)$ with the correlation function $\langle\eta(t_1)\eta(t_2)\rangle$, its characteristic functional is given by[97]

$$\begin{aligned}&\left\langle\exp\left[i\int_0^t {\rm d}t' p(t')\eta(t')\right]\right\rangle_\eta\\ &=\exp\left(-\frac{1}{2}\int_0^t {\rm d}t_1\int_0^t {\rm d}t_2 p(t_1)\langle\eta(t_1)\eta(t_2)\rangle p(t_2)\right).\end{aligned} \tag{42}$$

Using the above relation in eqn (37) for the thermal noise $\eta(t)$, we arrive at

$$\begin{aligned}P(x,t) =& \frac{1}{2\pi}\int {\rm d}q {\rm e}^{-iqx}{\rm e}^{-\xi_1^2(t)q^2-\xi_2^2(t)q^2}\left\langle {\rm e}^{iqk_I\int_0^t {\rm d}t_1\psi(t-t_1)\eta_{{\rm h},i}(t_1)}\right\rangle_{\eta_{{\rm h},i}(t_1)}\\ &\times\left\langle {\rm e}^{iqk_I\int_0^t {\rm d}t_1\psi(t-t_1)\eta_{{\rm c},i}(t_1)}\right\rangle_{\eta_{{\rm c},i}(t_1)},\end{aligned} \tag{43}$$

where

$$\begin{aligned}\xi_2^2(t) =& \frac{D_{\rm tr}{\rm e}^{-\alpha_1 t}}{2\alpha_1(\alpha_1^2-4\alpha_2)\alpha_2}[4\alpha_2\{\alpha_2+k_0(k_0-\alpha_1)\}\\ &+\left(\alpha_1^2-4\alpha_2\right)\left(\alpha_2+k_0^2\right){\rm e}^{\alpha_1 t}\\ &+\alpha_1\sqrt{\alpha_1^2-4\alpha_2}\left(\alpha_2-k_0^2\right)\sinh\left(\sqrt{\alpha_1^2-4\alpha_2}t\right)\\ &-\alpha_1\left\{\alpha_1\left(\alpha_2+k_0^2\right)-4\alpha_2 k_0\right\}\cosh\left(\sqrt{\alpha_1^2-4\alpha_2}t\right)\Big].\end{aligned} \tag{44}$$

Now let us consider the hot and cold particles as AOUPs (model II). So, by virtue of eqn (42), one can calculate the average over the active noises as

$$\begin{aligned}&\left\langle {\rm e}^{iqk_I\int_0^t {\rm d}t_1\psi(t-t_1)\eta_{{\rm h},i}(t_1)}\right\rangle_{\eta_{{\rm h},i}(t_1)}\\ &=\exp\left(-q^2k_I^2\frac{D_{\rm h}}{2\tau_{\rm h}}\int_0^t {\rm d}t_1\int_0^t {\rm d}t_2\psi(t-t_1)\right.\\ &\left.\times\,{\rm e}^{-\frac{|t_1-t_2|}{\tau_{\rm h}}}\psi(t-t_2)\right)=\exp\left(-q^2\xi_{31}^2(t)\right),\end{aligned} \tag{45}$$

where

$$\begin{aligned}&\xi_{31}^2(t)\\ &=\frac{D_{\rm h}k_I^2}{(\alpha_1^2-4\alpha_2)(\tau_{\rm h}(\alpha_1+\alpha_2\tau_{\rm h})+1)}\\ &\times\left[\frac{\alpha_1+\alpha_1^2\tau_{\rm h}-2\alpha_2\tau_{\rm h}}{2\alpha_2}-\frac{2}{\alpha_1}-\tau_{\rm h}+\frac{\sqrt{\alpha_1^2-4\alpha_2}\tau_{\rm h}^2{\rm e}^{-\frac{t}{\tau_{\rm h}}-\frac{\alpha_1 t}{2}}}{\tau_{\rm h}(\alpha_1-\alpha_2\tau_{\rm h})-1}\right.\\ &\times\left((\alpha_1\tau_{\rm h}+2)\sinh\left(\frac{1}{2}\sqrt{\alpha_1^2-4\alpha_2}t\right)\right.\\ &\left.\left.+\sqrt{\alpha_1^2-4\alpha_2}\tau_{\rm h}\cosh\left(\frac{1}{2}\sqrt{\alpha_1^2-4\alpha_2}t\right)\right)\right.\\ &-\frac{[\tau_{\rm h}(\alpha_1+\alpha_2\tau_{\rm h})+1]{\rm e}^{-\alpha_1 t}}{2\alpha_1\alpha_2(\tau_{\rm h}(\alpha_1-\alpha_2\tau_{\rm h})-1)}\\ &\times\left(\alpha_1\left(-\alpha_1+\alpha_1^2\tau_{\rm h}-2\alpha_2\tau_{\rm h}\right)\cosh\left(\sqrt{\alpha_1^2-4\alpha_2}t\right)\right.\\ &\left.\left.+\alpha_1\sqrt{\alpha_1^2-4\alpha_2}(\alpha_1\tau_{\rm h}-1)\sinh\left(\sqrt{\alpha_1^2-4\alpha_2}t\right)-2\alpha_2(\alpha_1\tau_{\rm h}-2)\right)\right].\end{aligned} \tag{46}$$

Similarly, one has $\left\langle {\rm e}^{iqk_I\int_0^t {\rm d}t_1\psi(t-t_1)\eta_{{\rm c},i}(t_1)}\right\rangle_{\eta_{{\rm c},i}(t_1)} = {\rm e}^{-q^2\xi_{32}^2(t)}$, where

$$\begin{aligned}&\xi_{32}^2(t)\\ &=\frac{D_{\rm c}k_I^2}{(\alpha_1^2-4\alpha_2)(\tau_{\rm c}(\alpha_1+\alpha_2\tau_{\rm c})+1)}\left[\frac{\alpha_1+\alpha_1^2\tau_{\rm c}-2\alpha_2\tau_{\rm c}}{2\alpha_2}-\frac{2}{\alpha_1}-\tau_{\rm c}\right.\\ &+\frac{\sqrt{\alpha_1^2-4\alpha_2}\tau_{\rm c}^2{\rm e}^{-\frac{t}{\tau_{\rm c}}-\frac{\alpha_1 t}{2}}}{\tau_{\rm c}(\alpha_1-\alpha_2\tau_{\rm c})-1}\left((\alpha_1\tau_{\rm c}+2)\sinh\left(\frac{1}{2}\sqrt{\alpha_1^2-4\alpha_2}t\right)\right.\\ &\left.\left.+\sqrt{\alpha_1^2-4\alpha_2}\tau_{\rm c}\cosh\left(\frac{1}{2}\sqrt{\alpha_1^2-4\alpha_2}t\right)\right)\right.\\ &-\frac{[\tau_{\rm c}(\alpha_1+\alpha_2\tau_{\rm c})+1]{\rm e}^{-\alpha_1 t}}{2\alpha_1\alpha_2(\tau_{\rm c}(\alpha_1-\alpha_2\tau_{\rm c})-1)}\\ &\times\left(\alpha_1\left(-\alpha_1+\alpha_1^2\tau_{\rm c}-2\alpha_2\tau_{\rm c}\right)\cosh\left(\sqrt{\alpha_1^2-4\alpha_2}t\right)\right.\\ &\left.\left.+\alpha_1\sqrt{\alpha_1^2-4\alpha_2}(\alpha_1\tau_{\rm c}-1)\sinh\left(\sqrt{\alpha_1^2-4\alpha_2}t\right)-2\alpha_2(\alpha_1\tau_{\rm c}-2)\right)\right].\end{aligned} \tag{47}$$

Using the above results, the PDF can be rewritten as

$$\begin{aligned}P(x,t) &= \frac{1}{2\pi}\int {\rm d}q{\rm e}^{-iqx}{\rm e}^{-\xi_1^2(t)q^2-\xi_2^2(t)q^2-\xi_3^2(t)q^2}\\ &=\sqrt{\frac{1}{4\pi\xi^2(t)}}\exp\left(-\frac{x^2}{4\xi^2(t)}\right),\end{aligned} \tag{48}$$

with

$$\xi_3^2(t) = N_{\rm h}\xi_{31}^2(t) + N_{\rm c}\xi_{32}^2(t), \tag{49}$$

and the variance is given by $2\xi^2(t)$,

$$\xi^2(t) = \xi_1^2 + \xi_2^2(t) + \xi_3^2(t). \tag{50}$$

For model I where $\eta_h(t)$ and $\eta_c(t)$ are taken as the Gaussian white noises, $\xi_3^2(t)$ can be computed by taking the limits $\tau_h \to 0$ and $\tau_c \to 0$. The result is

$$\xi_3^2(t) = [D_h N_h + D_c N_c] k_I^2 \frac{e^{-\alpha_1 t}}{2\alpha_1(\alpha_1^2 - 4\alpha_2)\alpha_2}\Big[4\alpha_2 + (\alpha_1^2 - 4\alpha_2)e^{\alpha_1 t} - \alpha_1\Big\{\sqrt{\alpha_1^2 - 4\alpha_2}\sinh\Big(\sqrt{\alpha_1^2 - 4\alpha_2}t\Big) + \alpha_1\cosh\Big(\sqrt{\alpha_1^2 - 4\alpha_2}t\Big)\Big\}\Big]. \quad (51)$$

Temporal behaviour of $\langle x^2(t)\rangle$ at short and long times

In the short-time limit, *i.e.*, for $t \to 0$, one has the following approximations: $\psi(t) \sim t$ and $\phi(t) \sim 1 - \alpha_1 t$, leading to $\xi_2^2(t=0) \sim D_{tr}t$, $\xi_3^2(t) \sim 0$ and $\xi_1^2(t) \sim \frac{D_{tr}}{2k}(1 - 2kt - jNk_I t)$ where $j = 1, 2$ for initial condition II and I, respectively. So the second moment of the displacement at $t = 0$ becomes $\langle x^2(t=0)\rangle = 2\lim_{t\to 0}\xi^2(t) = \frac{D_{tr}}{k} = \frac{T_{tr}}{\lambda}$. In the limit $t \to \infty$, the terms can be approximated as $\psi(t) \sim \phi(t) \sim 0$, $\xi_1^2(t) \sim 0$ and $\xi_2^2(t) \sim D_{tr}\frac{\alpha_2 + k_0^2}{2\alpha_1\alpha_2}$. For model I and II of active noise, one has $\xi_3^2(t) \sim \frac{[D_h N_h + D_c N_c]k_I^2}{2\alpha_1\alpha_2}$ and $\xi_3^2 \sim \frac{N_h D_h k_I^2(1+\alpha_1\tau_h)}{2\alpha_1\alpha_2(\tau_h(\alpha_1+\alpha_2\tau_h)+1)} + \frac{N_c D_c k_I^2(1+\alpha_1\tau_c)}{2\alpha_1\alpha_2(\tau_c(\alpha_1+\alpha_2\tau_c)+1)}$.

B Simulation details

We employ the Euler–Maruyama method to simulate the dynamics of the tracer as well as the active particles which are given by eqn (1a)–(1c). For the sake of simplicity, the tracer is considered to be interacting with only one hot and one cold particle, though the dynamical characteristics remain unchanged if it is coupled to more than one hot (and cold) particle. The simulations are performed over 2×10^3 trajectories with integration time step $\Delta t = 10^{-3}$ for total time $t = 100$. The initial positions of the tracer are sampled from the Boltzmann distribution of the form: $P(x_0) = e^{-\frac{k}{2D_{tr}}x_0^2}$, where $\lambda = 1.0$, $\gamma_{tr} = 2.0$, $T_{tr} = 50$, $k = \frac{\lambda}{\gamma_{tr}} = 0.5$ and $D_{tr} = \frac{T_{tr}}{\gamma_{tr}} = 25$. For active particles, their positions at $t = 0$ are taken as $x_h(0) = 0$ and $x_c(0) = 0$. Other parameters are $\lambda_0 = 1.0$, $\gamma_b = 1.0$ and $k_B = 1$. All the parameters are with their respective units given in Table 1.

C Fourier transform of the response function and autocorrelation

Taking the Fourier transform of eqn (1a)–(1c) defined as $\tilde{x}(\omega) = \frac{1}{2\pi}\int_{-\infty}^{+\infty} dt e^{i\omega t}x(t)$, one obtains the coupled equations

$$-i\omega\tilde{x}(\omega) = -k\tilde{x}(\omega) - \sum_{i=1}^{N_h} k_I(\tilde{x}(\omega) - \tilde{x}_{h,i}(\omega)) - \sum_{i=1}^{N_c} k_I(\tilde{x}(\omega) - \tilde{x}_{c,i}(\omega)) + \tilde{\eta}(\omega), \quad (52)$$

$$-i\omega\tilde{x}_h(\omega) = -k_0(\tilde{x}_h(\omega) - \tilde{x}(\omega)) + \tilde{\eta}_h(\omega), \quad (53)$$

$$-i\omega\tilde{x}_c(\omega) = -k_0(\tilde{x}_c(\omega) - \tilde{x}(\omega)) + \tilde{\eta}_c(\omega). \quad (54)$$

Rearranging the terms yields $\tilde{x}_h(\omega) = k_0\frac{\tilde{x}(\omega)}{k_0 - i\omega} + \frac{\tilde{\eta}_h(\omega)}{k_0 - i\omega}$ and $\tilde{x}_c(\omega) = k_0\frac{\tilde{x}(\omega)}{k_0 - i\omega} + \frac{\tilde{\eta}_c(\omega)}{k_0 - i\omega}$. With the use of $x_h(\omega)$ and $x_c(\omega)$, it further reduces to

$$\tilde{x}(\omega)\left[-i\omega + k + Nk_I - k_0\frac{Nk_I}{k_0 - i\omega}\right] = \sum_{i=1}^{N_h} k_I\frac{\tilde{\eta}_{h,i}(\omega)}{k_0 - i\omega} + \sum_{i=1}^{N_c} k_I\frac{\tilde{\eta}_{c,i}(\omega)}{k_0 - i\omega} + \tilde{\eta}(\omega). \quad (55)$$

The solution of $x(t)$ in Fourier domain can thus be recast as

$$\tilde{x}(\omega) = \sum_{i=1}^{N_h} k_I\frac{\tilde{\eta}_{h,i}(\omega)}{\mathbb{I}(\omega)} + \sum_{i=1}^{N_c} k_I\frac{\tilde{\eta}_{c,i}(\omega)}{\mathbb{I}(\omega)} + \tilde{\eta}(\omega)\frac{k_0 - i\omega}{\mathbb{I}(\omega)}, \quad (56)$$

where $\mathbb{I}(\omega) = -\omega^2 - i\omega(k_0 + k + Nk_I) + kk_0$. Using eqn (56), the autocorrelation function for position can be expressed as

$$\tilde{\mathbb{S}}_{xx}(\omega) = \langle\tilde{x}(\omega)\tilde{x}(-\omega)\rangle = \sum_{i=1}^{N_h} k_I^2\frac{\langle\tilde{\eta}_{h,i}(\omega)\tilde{\eta}_{h,i}(-\omega)\rangle}{\mathbb{I}(\omega)\mathbb{I}(-\omega)} + \sum_{i=1}^{N_c} k_I^2\frac{\langle\tilde{\eta}_{c,i}(\omega)\tilde{\eta}_{c,i}(-\omega)\rangle}{\mathbb{I}(\omega)\mathbb{I}(-\omega)} + \langle\tilde{\eta}(\omega)\tilde{\eta}(-\omega)\rangle\frac{k_0^2 + \omega^2}{\mathbb{I}(\omega)\mathbb{I}(-\omega)}. \quad (57)$$

For the thermal noise, the Fourier transform of autocorrelation can be computed as

$$\langle\tilde{\eta}(\omega)\tilde{\eta}(\omega')\rangle = \frac{1}{(2\pi)^2}\int_{-\infty}^{+\infty} dt_1\int_{-\infty}^{+\infty} dt_2 e^{i\omega t_1 + i\omega' t_2}\langle\eta(t_1)\eta(t_2)\rangle = 2D_{tr}\delta(\omega + \omega').$$

To find the response function in Fourier domain, one can use eqn (56) and write the change in position as $\langle\delta\tilde{x}(\omega)\rangle = \langle\tilde{x}(\omega)\rangle_f - \langle\tilde{x}(\omega)\rangle_0 = \tilde{\chi}(\omega)\tilde{f}_{ext}(\omega)$, where the Fourier transform of the response function is given by

$$\tilde{\chi}(\omega) = \frac{k_0 - i\omega}{\mathbb{I}(\omega)} = \frac{(k_0 - i\omega)\mathbb{I}(-\omega)}{\mathbb{I}(\omega)\mathbb{I}(-\omega)} = \frac{k(\omega^2 + k_0^2) + Nk_I\omega^2 + i\omega(k_0^2 + \omega^2 + Nk_0k_I)}{(\omega^2 - kk_0)^2 + \omega^2(k_0 + k + Nk_I)^2}. \quad (58)$$

For the case when the active particles are modelled as the AOUPs (model II), the Fourier transform of the noise correlation for the active forces given in eqn (5a) and (5b) can be found to be $\langle\tilde{\eta}_j(\omega)\tilde{\eta}_j(-\omega)\rangle = \frac{D_j}{\tau_j}\frac{2\tau_j}{1 + \omega^2\tau_j^2}$, where $j = h, c$. Therefore, the positional autocorrelation function given in eqn (57) can be

calculated for model II, and it reads

$$\tilde{\mathbb{S}}_{xx}(\omega) = \frac{2N_h k_I^2 D_h}{\mathbb{I}(\omega)\mathbb{I}(-\omega)} \frac{1}{1+\omega^2\tau_h^2} + \frac{2N_c k_I^2 D_c}{\mathbb{I}(\omega)\mathbb{I}(-\omega)} \frac{1}{1+\omega^2\tau_c^2} + 2D_{tr}\frac{k_0^2+\omega^2}{\mathbb{I}(\omega)\mathbb{I}(-\omega)}. \quad (59)$$

Taking $\tau_h \to 0$ and $\tau_c \to 0$ in the above equation, one can recover the autocorrelation function for model I, and the result is

$$\tilde{\mathbb{S}}_{xx}(\omega) = \langle \tilde{x}(\omega)\tilde{x}(-\omega)\rangle = \frac{2N_h k_I^2 D_h}{\mathbb{I}(\omega)\mathbb{I}(-\omega)} + \frac{2N_c k_I^2 D_c}{\mathbb{I}(\omega)\mathbb{I}(-\omega)} + 2D_{tr}\frac{k_0^2+\omega^2}{\mathbb{I}(\omega)\mathbb{I}(-\omega)}. \quad (60)$$

For the MOUP case as discussed at the end of Section 2.1.2, $\tilde{\mathbb{S}}_{xx}(\omega)$ can be calculated from eqn (59) in a straightforward manner just by replacing D_h and D_c with $G_h\tau_h$ and $G_c\tau_c$, respectively. So the autocorrelation function for the MOUP case is given by

$$\tilde{\mathbb{S}}_{xx}(\omega) = \frac{2N_h k_I^2 G_h}{\mathbb{I}(\omega)\mathbb{I}(-\omega)} \frac{\tau_h}{1+\omega^2\tau_h^2} + \frac{2N_c k_I^2 G_c}{\mathbb{I}(\omega)\mathbb{I}(-\omega)} \frac{\tau_c}{1+\omega^2\tau_c^2} + 2D_{tr}\frac{k_0^2+\omega^2}{\mathbb{I}(\omega)\mathbb{I}(-\omega)}. \quad (61)$$

Acknowledgements

We thank A. G. Cherstvy for stimulating discussions and for critical reading of the revised manuscript. Funding from the German Science Foundation (DFG grant ME 1535/13-1) is acknowledged.

Notes and references

1 D. Mizuno, C. Tardin, C. F. Schmidt and F. C. MacKintosh, *Science*, 2007, **315**, 370.
2 E. Barkai, Y. Garini and R. Metzler, *Phys. Today*, 2012, **65**, 29.
3 K. Nørregaard, R. Metzler, C. M. Ritter, K. Berg-Sørensen and L. B. Oddershede, *Chem. Rev.*, 2017, **117**, 4342.
4 É. Fodor, M. Guo, N. S. Gov, P. Visco, D. A. Weitz and F. Van Wijland, *Europhys. Lett.*, 2015, **110**, 48005.
5 R. Kubo, M. Toda and N. Hashitsume, *Statistical Physics II: non-equilibrium Statistical Mechanics*, Springer, Berlin, 2012.
6 R. Zwanzig, *Non-equilibrium Statistical Mechanics*, Oxford University Press, Oxford, 2001.
7 U. Seifert, *Rep. Prog. Phys.*, 2012, **75**, 126001.
8 A. W. Lau, B. D. Hoffman, A. Davies, J. C. Crocker and T. C. Lubensky, *Phys. Rev. Lett.*, 2003, **91**, 198101.
9 H. Turlier, D. A. Fedosov, B. Audoly, T. Auth, N. S. Gov, C. Sykes, J. F. Joanny, G. Gompper and T. Betz, *Nat. Phys.*, 2016, **12**, 513.
10 H. Seyforth, M. Gomez, W. B. Rogers, J. L. Ross and W. W. Ahmed, *Phys. Rev. Res.*, 2022, **4**, 023043.
11 L. F. Cugliandolo, J. Kurchan and L. Peliti, *Phys. Rev. E: Stat., Nonlinear, Soft Matter Phys.*, 1997, **55**, 3898.
12 B. Abou and F. Gallet, *Phys. Rev. Lett.*, 2004, **93**, 160603.
13 J. Dzubiella, H. Löwen and C. Likos, *Phys. Rev. Lett.*, 2003, **91**, 248301.
14 M. Krüger and M. Fuchs, *Phys. Rev. Lett.*, 2009, **102**, 135701.
15 R. Gomez-Solano, A. Petrosyan, S. Ciliberto, R. Chetrite and K. Gawedski, *Phys. Rev. Lett.*, 2009, **103**, 040601.
16 J. Mehl, V. Blickle, U. Seifert and C. Bechinger, *Phys. Rev. E: Stat., Nonlinear, Soft Matter Phys.*, 2010, **82**, 032401.
17 C. Bechinger, R. Di Leonardo, H. Löwen, C. Reichhardt, G. Volpe and G. Volpe, *Rev. Mod. Phys.*, 2016, **88**, 045006.
18 J. O'Byrne, Y. Kafri, J. Tailleur and F. van Wijland, *Nat. Rev. Phys.*, 2022, **4**, 67.
19 P. Martin, A. J. Hudspeth and F. Jülicher, *Proc. Natl. Acad. Sci. U. S. A.*, 2001, **98**, 14380.
20 D. Mizuno, R. Bacabac, C. Tardin, D. Head and C. F. Schmidt, *Phys. Rev. Lett.*, 2009, **102**, 168102.
21 L. Dinis, P. Martin, J. Barral, J. Prost and J. F. Joanny, *Phys. Rev. Lett.*, 2012, **109**, 160602.
22 T. Harada and S.-I. Sasa, *Phys. Rev. Lett.*, 2005, **95**, 130602.
23 T. Speck and U. Seifert, *Europhys. Lett.*, 2006, **74**, 391.
24 A. V. Chechkin and R. Klages, *J. Stat. Mech.: Theory Exp.*, 2009, L03002.
25 A. V. Chechkin, F. Lenz and R. Klages, *J. Stat. Mech.: Theory Exp.*, 2012, L11001.
26 É. Fodor, C. Nardini, M. E. Cates, J. Tailleur, P. Visco and F. van Wijland, *Phys. Rev. Lett.*, 2016, **117**, 038103.
27 S. Dal Cengio, D. Levis and I. Pagonabarraga, *Phys. Rev. Lett.*, 2019, **123**, 238003.
28 N. Xu and C. S. O'Hern, *Phys. Rev. Lett.*, 2005, **94**, 055701.
29 M. D. El Alaoui Faris, D. Lacoste, J. Pécréaux, J. F. Joanny, J. Prost and P. Bassereau, *Phys. Rev. Lett.*, 2009, **102**, 038102.
30 E. Ben-Isaac, Y. Park, G. Popescu, F. L. Brown, N. S. Gov and Y. Shokef, *Phys. Rev. Lett.*, 2011, **106**, 238103.
31 T. Betz and C. Sykes, *Soft Matter*, 2012, **8**, 5317.
32 F. Y. Chu, S. C. Haley and A. Zidovska, *Proc. Natl. Acad. Sci. U. S. A.*, 2017, **114**, 10338.
33 C. Maggi, M. Paoluzzi, N. Pellicciotta, A. Lepore, L. Angelani and R. Di Leonardo, *Phys. Rev. Lett.*, 2014, **113**, 238303.
34 D. Levis and L. Berthier, *Europhys. Lett.*, 2015, **111**, 60006.
35 K. Goswami, *Phys. Rev. E*, 2019, **99**, 012112.
36 D. Krapf, N. Lukat, E. Marinari, R. Metzler, G. Oshanin, C. Selhuber-Unkel, A. Squarcini, L. Stadler, M. Weiss and X. Xu, *Phys. Rev. X*, 2019, **9**, 011019.
37 O. Vilk, E. Aghion, R. Nathan, S. Toledo, R. Metzler and M. Assaf, *J. Phys. A: Math. Theor.*, 2022, **55**, 334004.
38 É. Fodor, K. Kanazawa, H. Hayakawa, P. Visco and F. Van Wijland, *Phys. Rev. E: Stat., Nonlinear, Soft Matter Phys.*, 2014, **90**, 042724.
39 T. Hiraiwa and R. R. Netz, *Europhys. Lett.*, 2018, **123**, 58002.
40 R. Zwanzig, *J. Stat. Phys.*, 1973, **9**, 215.
41 R. R. Netz, *J. Chem. Phys.*, 2018, **148**, 185101.

42 E. W. Burkholder and J. F. Brady, *J. Chem. Phys.*, 2019, **150**, 184901.
43 K. Goswami, *Phys. A*, 2019, **525**, 223.
44 S. Chaki and R. Chakrabarti, *Phys. A*, 2019, **530**, 121574.
45 S. Eldeen, R. Muoio, P. Blaisdell-Pijuan, N. La, M. Gomez, A. Vidal and W. W. Ahmed, *Soft Matter*, 2020, **16**, 7202.
46 M. Knežević and H. Stark, *New J. Phys.*, 2020, **22**, 113025.
47 C. Jones, M. Gomez, R. M. Muoio, A. Vidal, R. A. Mcknight, N. D. Brubaker and W. W. Ahmed, *Phys. Rev. E*, 2021, **103**, 032403.
48 K. Goswami, *Phys. A*, 2021, **566**, 125609.
49 J. Shea, G. Jung and F. Schmid, *Soft Matter*, 2022, **18**, 6965.
50 S. M. J. Khadem, R. Klages and S. H. Klapp, *Phys. Rev. Res.*, 2022, **4**, 043186.
51 F. Jülicher, K. Kruse, J. Prost and J. F. Joanny, *Phys. Rep.*, 2007, **449**, 3.
52 C. P. Broedersz and F. C. MacKintosh, *Rev. Mod. Phys.*, 2014, **86**(3), 995.
53 S. Scott, M. Weiss, C. Selhuber-Unkel, Y. F. Barooji, A. Sabri, J. T. Erler, R. Metzler and L. B. Oddershede, *Phys. Chem. Chem. Phys.*, 2023, **25**, 1513.
54 G. H. Koenderink, Z. Dogic, F. Nakamura, P. M. Bendix, F. C. MacKintosh, J. H. Hartwig, T. P. Stossel and D. A. Weitz, *Proc. Natl. Acad. Sci. U. S. A.*, 2009, **106**, 15192.
55 T. Toyota, D. A. Head, C. F. Schmidt and D. Mizuno, *Soft Matter*, 2011, **7**, 3234.
56 B. Stuhrmann, M. Soares e Silva, M. Depken, F. C. MacKintosh and G. H. Koenderink, *Phys. Rev. E: Stat., Nonlinear, Soft Matter Phys.*, 2012, **86**, 020901.
57 Y. Park, C. A. Best, T. Auth, N. S. Gov, S. A. Safran, G. Popescu, S. Suresh and M. S. Feld, *Proc. Natl. Acad. Sci. U. S. A.*, 2010, **107**(4), 1289.
58 A. Zidovska, D. A. Weitz and T. J. Mitchison, *Proc. Natl. Acad. Sci. U. S. A.*, 2013, **110**, 15555.
59 D. Saintillan, M. J. Shelley and A. Zidovska, *Proc. Natl. Acad. Sci. U. S. A.*, 2018, **115**, 11442.
60 R. Bruinsma, A. Y. Grosberg, Y. Rabin and A. Zidovska, *Biophys. J.*, 2014, **106**, 1871.
61 G. Fudenberg, M. Imakaev, C. Lu, A. Goloborodko, N. Abdennur and L. A. Mirny, *Cell Rep.*, 2016, **15**, 2038.
62 C. Maes, *Phys. Rev. Lett.*, 2020, **125**, 208001.
63 M. Wang, K. Zinga, A. Zidovska and A. Y. Grosberg, *Soft Matter*, 2021, **17**, 9528.
64 O. Granek, Y. Kafri and J. Tailleur, *Phys. Rev. Lett.*, 2022, **129**, 038001.
65 S. Joo, X. Durang, O. C. Lee and J.-H. Jeon, *Soft Matter*, 2020, **16**, 9188.
66 J.-H. Jeon, N. Leijnse, L. B. Oddershede and R. Metzler, *New J. Phys.*, 2013, **15**, 045011.
67 A. Godec, M. Bauer and R. Metzler, *New J. Phys.*, 2014, **16**, 092002.
68 Y. Kim, S. Joo, W. K. Kim and J.-H. Jeon, *Macromolecules*, 2022, **55**, 7136.
69 L. Theeyancheri, R. Sahoo, P. Kumar and R. Chakrabarti, *ACS Omega*, 2022, **7**, 33637.
70 P. Kumar and R. Chakrabarti, *Phys. Chem. Chem. Phys.*, 2023, **25**, 1937.
71 H. Han, S. Joo, T. Sakaue and J.-H. Jeon, *J. Chem. Phys.*, 2023, **159**, 024901.
72 A. Y. Grosberg and J. F. Joanny, *Phys. Rev. E: Stat., Nonlinear, Soft Matter Phys.*, 2015, **92**, 032118.
73 R. R. Netz, *Phys. Rev. E*, 2020, **101**, 022120.
74 M. Wang and A. Y. Grosberg, *Phys. Rev. E*, 2020, **101**, 032131.
75 E. Ilker, M. Castellana and J. F. Joanny, *Phys. Rev. Res.*, 2021, **3**, 023207.
76 S. Ramaswamy, *J. Stat. Mech.: Theory Exp.*, 2017, 054002.
77 K. Goswami, *Phys. Rev. E*, 2022, **105**, 044123.
78 S. Ramaswamy, *Annu. Rev. Condens. Matter Phys.*, 2010, **1**, 323.
79 D. B. Kearns, *Nat. Rev. Microbiol.*, 2010, **8**, 634.
80 N. Fakhri, A. D. Wessel, C. Willms, M. Pasquali, D. R. Klopfenstein, F. C. MacKintosh and C. F. Schmidt, *Science*, 2014, **344**, 1031.
81 C. De Pascalis and S. Etienne-Manneville, *Mol. Biol. Cell*, 2017, **28**, 1833.
82 J. Shin, A. G. Cherstvy, W. K. Kim and R. Metzler, *New J. Phys.*, 2015, **17**, 113008.
83 J. Shin, A. G. Cherstvy, W. K. Kim and V. Zaburdaev, *Phys. Chem. Chem. Phys.*, 2017, **19**, 18338.
84 H. Chen, M. Levo, L. Barinov, M. Fujioka, J. B. Jaynes and T. Gregor, *Nat. Genet.*, 2018, **50**, 1296.
85 K. Goswami, S. Chaki and R. Chakrabarti, *J. Phys. A: Math. Theor.*, 2022, **55**, 423002.
86 K. Goswami and R. Chakrabarti, *Soft Matter*, 2022, **18**, 2332.
87 A. Solon and J. M. Horowitz, *J. Phys. A: Math. Theor.*, 2022, **55**, 184002.
88 I. Santra, *J. Phys. Complex.*, 2023, **4**, 015013.
89 C. A. Guevara-Valadez, R. Marathe and J. R. Gomez-Solano, *Phys. A*, 2023, **609**, 128342.
90 S. Ye, P. Liu, F. Ye, K. Chen and M. Yang, *Soft Matter*, 2020, **16**, 4655.
91 K. Goswami and K. L. Sebastian, *J. Stat. Mech.: Theory Exp.: Theory Exp.*, 2019, 083501.
92 K. Goswami and R. Metzler, *J. Phys. Complex.*, 2023, **4**, 025005.
93 J.-H. Jeon, V. Tejedor, S. Burov, E. Barkai, C. Selhuber-Unkel, K. Berg-Sørensen, L. B. Oddershede and R. Metzler, *Phys. Rev. Lett.*, 2011, **106**, 048103.
94 S. C. Takatori, R. De Dier, J. Vermant and J. F. Brady, *Nat. Commun.*, 2016, **7**, 10694.
95 F. Schmidt, H. Šípová-Jungová, M. Käll, A. Würger and G. Volpe, *Nat. Commun.*, 2021, **12**, 1902.
96 H. Risken, *The Fokker-Planck Equation*, Springer, Berlin, 1989.
97 N. G. Van Kampen, *Stochastic processes in physics and chemistry*, North-Holland, Amsterdam, 1991.
98 S. Toyabe, H. R. Jiang, T. Nakamura, Y. Murayama and M. Sano, *Phys. Rev. E: Stat., Nonlinear, Soft Matter Phys.*, 2007, **75**, 011122.

99 K. Berg-Sørensen and H. Flyvbjerg, *Rev. Sci. Instrum.*, 2004, **75**, 594.
100 A. G. Cherstvy, S. Thapa, Y. Mardoukhi, A. V. Chechkin and R. Metzler, *Phys. Rev. E*, 2018, **98**, 022134.
101 S. N. Majumdar and G. Oshanin, *J. Phys. A: Math. Theor.*, 2018, **51**, 435001.
102 A. Squarcini, A. Solon and G. Oshanin, *New J. Phys.*, 2022, **24**, 013018.
103 F. Ginot, J. Caspers, M. Krüger and C. Bechinger, *Phys. Rev. Lett.*, 2022, **128**, 028001.
104 A. Kamenev, *Field theory of non-equilibrium systems*, Cambridge University Press, Cambridge, 2011.